Petrography, mineral chemistry, fluid inclusion microthermometry and Re-Os geochronology of the Küre Volcanogenic Massive Sulfide Deposit (Central Pontides, Northern Turkey)

Mehmet Akbulut[a,] *, Tolga Oyman[a], Mustafa Çiçek[a], David Selby[b], İsmet Özgenç[a,†], Murat Tokçaer[a]

[a]Dokuz Eylul University, Department of Geological Engineering, Buca, Izmir,TR-35160,Turkey

[b]Durham University, Department of Earth Sciences, Durham, DH1 3LE, UK

[†] Emeritus

* Corresponding Author: Mehmet AKBULUT, Dokuz Eylul University, Department of Geological Engineering, Buca, Izmir, TR-35160, Turkey

E-mail: makbulut@deu.edu.tr; mehmet.akbulut@deu.edu.tr; Tel.: +90 232 3017349; Fax: +90 232 4531129.

Abstract

The Re-Os isotopic system is applied for the first time to the sulfide ores and the overlying black-shales at the Küre volcanogenic massive sulfide deposit of the Central Pontides, Northern Turkey. The ore samples collected include predominantly pyrite, accompanied by chalcopyrite, sphalerite and other species. Massive ore is almost free of gangues, whereas the stockwork ore includes quartz and calcite gangue. The composition of sphalerite is similar to ancient and modern massive sulfide mineralizations globally. Microthermometric studies from quartz from the stockwork ore has shown two populations of two-phase fluid inclusions with vapor/liquid ratios between 4 to 28%, low to intermediate T_h (161.5-317.0°C) and low salinities (0.9-5 wt % NaCl equiv.) which are mostly in good agreement with the ranges for volcanogenic massive sulfide mineralizations. These studies also suggest a H_2O-$CaCl_2$-KCl-$MgCl_2$ ore-forming fluid system in a shallower subsurface near the seafloor vents. The Re-Os dating of the LLHR sulfides yield a nominal depositional age of upper Toarcian for the massive sulfide mineralization. Two largely different model ages obtained are attributed to other pyrite crystallization events prior to and postdating the main sulfide deposition. Some lower homogenization temperatures (<200°C) from the quartz of the stockwork may also similarly be related to the post-VMS events. It is concluded that a submarine volcanic extrusion episode has continued until upper Toarcian in the Küre Basin, when it has entered a stagnation period that allowed the discharge of hydrothermally circulated sulfide-laden fluids from the seafloor vents. This age data promotes the paleotectonic models interpreting the Küre Basin as a Permian-early Jurassic marginal back-arc basin of the Devonian-Triassic Karakaya Ocean. The Re-Os data from the overlying black-shale provide a glimpse to the initial Os isotope ratio of the water column at the time of the sedimentation (0.45-0.46 for 180 Ma). The lack of common Os from the sulfides does not let us to infer a source of Os and initial $^{187}Os/^{188}Os$ ratios from the black shale are not statistically robust to make a significant deduction. A further detailed study on the isotopic composition of the black shale strata may help us to make an apporach to the Os source(s) in the deposition environment of the Küre VMS deposit.

Keywords: Re-Os geochronology, low level highly radiogenic sulfide, black shale, Cyprus-type massive sulfide deposits, Küre, Central Pontides

1. Introduction

Volcanogenic massive sulfide (VMS) deposits range from lens shaped to sheet-like bodies of polymetallic massive sulfide accumulations that form at or near the seafloor in submarine volcanic environments by introduction of metal-enriched fluids associated with seafloor hydrothermal convection (cf. Galley et al., 2007). To classify the VMS deposits worldwide, several methods/schemes have been proposed generally considering using one or more of the following three criteria: the metal contents (e.g., such as Cu- Zn, Zn-Cu and Zn-Pb-Cu subtypes; Franklin et al, 1981 ; Large, 1992; Franklin et al, 2005), host-rock lithologies (e.g., mafic-felsic-bimodal volcanic and/or siliciclastic rocks; Piercey, 2010; 2011) and the tectonic settings (e.g., extensional and/or compressional regimes related to oceanic rifting-spreading, island-arc formation;cf. Misra, 2000 and references therein). One of the oldest and well-known classification schemes present a combination of the host-lithology and the tectonic setting (e.g., Sawkins, 1976) in which the VMS deposits are sub-divided in Kuroko-, Cyprus-, and Besshi-type deposits (cf. Pirajno, 2009). Recently, the scheme by Barrie and Hannington (1999) and Franklin et al. (2005) that classifies the VMS deposits according to their host lithologies as: back-arc mafic, bimodal-mafic, pelitic-mafic, bimodal-felsic, felsic-siliciclastic and hybrid bimodal-felsic (cf. Galley et al., 2007) groups is well-accepted and used as a standard. However, studies on the Turkish VMS deposits generally uses the scheme by Sawkins (1976) and subdivided the VMS deposits of Turkey mainly into Kuroko- and Cyprus-types (cf. Yiğit, 2006). As type conversion of these Turkish VMS deposits would be a subject of another detailed study, we will continue with the current usage of Sawkins (1976) classification for Turkish VMS deposits hereafter.

The Kuroko-type deposits of Turkey (including Murgul, Cerattepe, Çayeli, Lahanos) that are accompanied by several porphyry Cu-Au mineralizations, are mainly located in the Eastern Pontides segment lying along northeastern Turkey (Fig. 1a). These deposits are located in felsic lavas and pyroclastics of calc-alkaline submarine volcanism. The occurrence of these deposits are usually attributed to the formation of the Late Cretaceous magmatic arc in the region. The Cyprus-type VMS deposits of Turkey, related to mafic submarine rocks (usually tholeiitic pillow lavas) on the contrary, are mainly concentrated in the Southern Anatolian Ophiolite Belt (Fig. 1a) that is interpreted as an eastern extension of the Troodos Massif (Cyprus) suture zone (Erler, 1984; Yiğit, 2006) again formed during the closure of the Tethys Ocean. Most important examples of this Cyprus-type VMS in this region are the Ergani and Madenköy Cu deposits. The Küre VMS deposit represents the sole Cyprus-type VMS occurrence, standing alone in the Central Pontides, just west of the Kuroko-type and porphyry deposits of the Eastern Pontides (Fig. 1a). The deposit is located in the Küre ophiolite which is considered as a remnant of a back-arc ocean that opened during the pre-Lias (Lower Jurassic) and closed in the early Dogger (Middle Jurassic) as part of the Tethyan realm (Sarıfakıoğlu et al., 2013).

The Küre VMS Deposit comprises several VMS occurrences; namely the Aşıköy, Kızılsu, Toykondu, Bakibaba, and Mağaradoruk mineralizations (Fig. 2; cf. Altun et al., 2015). The copper rich-massive sulfide ore bodies in the Küre region, mainly of the Bakibaba area, had been mined throughout the ancient history of the Anatolia. However, modern geological mapping and prospecting studies had been initiated shortly after the foundation of the Republic of Turkey and resulted in the exploration of the Aşıköy and Kızılsu areas and some virgin parts of the Bakibaba area (cf. Nikitin, 1926; Kovenko, 1944; Güner, 1980). The mining and prospecting continued sporadically by the governmental authorities (Maden Tetkik ve Arama Genel Müdürlüğü, Etibank, Karadeniz Bakır İşletmeleri) until 2004. Several deposits are currently being exploited by the Eti Bakır Joint-Stock Corporation, a subsidiary body of the Cengiz Holding (Turkey). Previous studies have documented the geology, geochemistry, mining geology, and ore paragenesis of many of the areas (e.g., Nikitin, 1926;

Kovenko, 1944; Güner, 1980; Çağatay et al., 1980; Pehlivanoğlu, 1985; Ustaömer and Robertson, 1994; Çakır, 1995; Kuşçu and Erler, 2002; Çakır et al., 2006; Altun et al., 2015); However, there is a lack of direct radiometric dating of the sulfides that comprise the mineralization of these VMS systems.

The age of ore deposition in a mineral deposit is one of the most important data that enlighten the history of the ore formation and its tectonic history. However, the ore deposition ages in VMS deposits are generally poorly constrained by indirect radiometric dating methods (e.g., ^{40}Ar-^{39}Ar, Rb-Sr, Sm-Nd) of the heavily altered and sometimes metamorphosed volcanic host rocks, and/or by the paleontological data from the sedimentary strata (cf. Hou et al., 2003). All of these methods concentrate on the silicate-gangue mineralogy of the host rock or the fossils, but not the ore. Thus, recent developments in direct dating of the sulfide phases have opened a new window of opportunity. The relatively new and continuously developing Re-Os method is nowadays considered as a powerful tool for radiometric dating of the sulfide phases as both of these elements present siderophile and chalcophile nature and tend to enrich in sulfide minerals (e.g., Walker et al., 1994; Suzuki et al., 1996; Mathur et al., 1999; Stein et al., 2000; Hannah et al., 2004; Morelli et al., 2005; Kato et al., 2009; Selby et al., 2009; Nozaki et al., 2010). The method is principally optimal in dating molybdenite (MoS_2) bearing Mo-Cu hydrothermal systems owing to the high Re enrichment (ppm) and only radiogenic Os in molybdenite. However, lately the method has been successfully applied to low Re and Os bearing (ppb and ppt, respectively) sulfide phases such as pyrite and arsenopyrite (cf. Arne et al., 2001; Stein et al., 2000; Liu et al., 2004; Yu et al., 2005; Selby et al., 2009; Guo et al., 2011) in VMS systems (e.g.; Terakado, 2001a, 2001b; Hou et al., 2003; Nozaki et al., 2010, 2014). These sulfides are mainly termed as “low-level highly radiogenic” (LLHR) sulfides (Stein et al., 2000) and provide a precise Re-Os dating tool in the absence of molybdenite, as they can include little or no initial Os content (Kerr and Selby, 2010). While pyrite and arsenopyrite are accepted as reliable, sphalerite is mainly considered as an unreliable media for LLHR sulfide Re-Os geochronology (cf. Morelli et al., 2004; Morelli et al., 2005; Kerr and Selby, 2010). The Re-Os dating is also an important tool in dating of the organic material-rich black-shales (e.g., Ravizza and Turekian, 1989; Ravizza et al., 1991; Cohen et al., 1999; 2004; Singh et al., 1999; Creaser et al., 2002; Selby and Creaser, 2003; Hannah et al., 2004; Fu et al., 2008). The method is especially very useful when the fossil distribution is limited and/or unclear (e.g., Kendall et al., 2006; Zhu et al., 2010). Re and Os are mainly included in sulfides and organic materials of the mud deposited in anoxic or euxinic marine environments, with the decay of ^{187}Re to ^{187}Os providing a radiometric clock that records the time of shale deposition (Hannah et al., 2008).

As the Küre VMS deposit in northern Turkey has a unique lithostratigraphy including huge pyrite-rich massive sulfide lenses that are constrained by the organic matter-rich black shale-sandstone alternations and pillow lavas, this geological setting provides one of the locations for applying the Re-Os isotope system. In this study, we present the first Re-Os isotopic data from both the pyrite and the black-shale of the Küre VMS deposit to constrain the age of main sulfide deposition and understand the depositional environment. In addition, we also present mineralogical and microthermometric data. With these new data, we further contribute to the origin of the Küre VMS mineralization and the understanding on the evolutionary history of its depositional environment.

2. Geological Setting

The Küre VMS deposit is located 61 km north of the Kastamonu City (central northern part of the Turkey, Figs. 1a and b) in the central part of the Pontides of the Tethyside system. The Pontides is an east-west trending orogenic belt located at the northernmost part of Turkey that comprise the Cimmeride and Alpide orogenic events in the Mediterranean realm related to the closure and opening of the Paleo- and Neo-Tethyan oceanic basins, respectively (cf. Yılmaz et al., 1997). The Pontides is generally divided in three main sectors; the western, the central, and the eastern Pontides.

The Küre Complex, located in the central Pontides, is defined as a thick wedge of late Palaeozoic-early Mesozoic mainly siliciclastic sediments interleaved with a dismembered ophiolite, named the Küre Ophiolite (Ustaömer and Robertson, 1994; Figs. 2a and 2b). The Küre Ophiolite comprises the Akgöl Group, İpsinler Basalt of the Küre Ocean Unit and the Elekdağ Ophiolite (cf. Kozur et al., 2000 and the references therein) and hosts the Küre VMS deposit. It is mainly interpreted as a metamorphosed and dismembered ophiolitic assemblage created by the geodynamics of the Paleo-Tethyan Ocean (e.g., Şengör et al., 1984; Ustaömer and Robertson, 1994; 1997; Yiğitbaş et al., 1999; 2004). The Küre Ophiolite mainly comprises serpentinized tectonites (harzburgite to dunite), intrusive gabbro and lherzolites, and spilitic basalts and diabase (e.g., Çakır, 1995; Terzioğlu et al., 2000; Çakır et al., 2006; Fig. 2). The tectonites, basalts and siliciclastic sedimentary rocks of the Küre Complex are mainly cross-cut by isolated diabase dykes, with the true sheeted dyke complex cross-cutting the isotropic microgabbros of the assemblage (e.g., Ustaömer and Robertson, 1993, 1994; Çakır et al., 2006). Terzioğlu et al. (2000) and Kozur et al (2000) also indicate existence of a small amount of trondhjemite-granophyres and altered plagiogranites in the complex. All of these units are intruded by Middle Jurassic granitoids-dacitic dikes (Boztuğ et al., 1995; Yılmaz, 1980; Kuşçu and Erler, 2002), and uncomformably covered by Middle-Late Jurassic basal conglomerates that are overlain by Late Jurassic limestones (e.g., Güner, 1980; Pehlivanoğlu, 1985; Aydın et al., 1986;Ustaömer and Robertson, 1994; Çakır, 1995; Çakır et al., 2006; Figs. 2a and b).

Owing to the extensive tectonism, the contacts of the Küre Complex rocks are generally disrupted and primary ophiolitic succession is missing. The tectonites are found thrusted over the basaltic and siliciclastic sedimentary rocks; likewise the basalts are commonly thrusted onto their siliciclastic sedimentary cover (cf. Çakır, 1995; Çakır et al., 2006). However, there are localities where the primary contact relations are observable (see below).

The basalts consist of massive to pillow lavas and hyaloclastites, and are covered conformably by a “shale-sandstone” (cf. Çakır, 1995; Çakır et al., 2006) or “black shale-subgraywacke” unit (Ketin and Gümüş, 1963; Güner, 1980; Kuşçu and Erler, 2002). This bottom to top original contact relationships between the basalt, the ore and the overlying sedimentary cover is only preserved locally at the Aşıköy mine area (cf. Çakır et al., 2006; Altun et al., 2015). Basaltic flow intercalations are common in the lower levels of the black shale-subgraywacke unit and vice versa (e.g., Tüysüz, 1986; Pehlivanoğlu, 1985), suggesting contemporaneous deposition of the lower segment of the black shales and the upper segment of the basalts (e.g., Çakır, 1995) in their original depositional setting. The ore bodies and their adjacent lithologies are steeply tilted (60-85°) and locally deformed, as seen by the black shale-subgraywacke and the pillow lava contact at the batters and berms of Bakibaba open pit (Fig. 3) and is also reported by Altun et al. (2015). According to Ustaömer and Robertson (1995), the upper contacts of the basalts with the sedimentary cover are commonly undeformed sedimentary and conformable contacts. These records of undeformed segments in the basalt-shale contacts, both at the surface and the drifts in the Bakibaba region, support a primary sedimentary and late stage tectonic character for the contacts probably related to the different rheological behavior of these lithologies during the emplacement of the Küre Complex (cf. Çakır, 1995).

The pillow lavas of the basaltic sequence gradationally changes into non pillowed, massive flows downwards, and the well-developed pillows decrease successively upwards, with the increasing hyaloclastites towards the black shale-subgraywacke contacts (cf. Güner, 1980; also see Fig. 2b). The primary mineralogy of the basalts comprises small lath-shaped (somewhat microlitic) plagioclase, interstitial clinopyroxene and opaque phases accompanied by chlorite and secondary amphibole after clinopyroxene. Ophitic-subophitic and/or variolitic textures are common in basalts (e.g., Figs. 4a and b). Güner (1980) indicates that the whole basaltic sequence has been subjected to considerable hydrothermal alteration. Indeed, an advanced chloritic alteration is especially common in the basalts adjacent to the massive sulfide lenses. The mafic phases are almost totally replaced by the chlorite and plagioclase is generally absent (Figs. 4c, d, e, f) being preserved only in some samples as thin laths of plagioclases (Fig. 4d). Secondary quartz and calcite are ubiquitous as infills and veinlets. The subgraywacke of the overlaying black shale-subgraywacke unit includes quartz, feldspar, rock fragments, chert and opaque phases embedded in a matrix of sericite, chlorite and limonite, whereas the almost unfossiliferous and very fine grained black shale is composed of illite, quartz, chlorite, siderite, and muscovite with accessory opaque phases (cf. Güner, 1980; Altun et al., 2015 and references therein).

The Küre VMS deposits contain massive, stockwork and disseminated ore, the former mainly located along the faults and contact planes between the basaltic lava (İpsinler Basalt) and the siliciclastic sedimentary rocks (Akgöl Group/Formation; Fig. 2). The originally uppermost basaltic lavas seems to be mostly overlain by massive sulfide ore bodies. The bun-like or loaf-shaped masses of high grade massive sulfide are dominantly pyrite and chalcopyrite, and are commonly underlain by stockworks and disseminated pyrite-rich sulfides, quartz and carbonates (cf., Güner, 1980; Kuşçu and Erler, 2002; Altun et al., 2015). Previous studies report that the chalcopyrite rich segment of the ore body is controlled by pre-existing faults (e.g., Bailey et al., 1966; Kuşçu and Erler, 2002). Kuşçu and Erler (2002) described cataclastic, thermal-annealing and fracture-filling textures in the pyrites of the massive sulfide mineralization interpreting deformational and late deformational stages of prograde metamorphism at greenschist (or even amphibolite) facies conditions, probably related to regional thrusting and folding of the Küre ophiolite. They also note that their observation is in good agreement with observations of Aydın et al. (1986), who report the metamorphosed nature of the black shale-subgraywacke unit at greenschist facies conditions, indicating that the Küre VMS was also metamorphosed at this facies conditions.

The Aşıköy deposit contains 11.8 million tonnes of pyrite ore with average grades of 1.69% Cu and 39.41% S (e.g., Yiğit, 2011), whereas the Bakibaba deposit contains 1.5 million tonnes of ore comprising average grades of 3.42% Cu and 43.49% S (Demirbaş and Ağaoğlu, 1980; Çağatay et al., 1980). Co, Au and Ag grades reported from both deposits are 0.3%, 2.48 g/t and 10 g/t, respectively (cf. Çağatay et al., 1980; Yiğit, 2011). The much smaller, but more Cu-rich Toykondu deposit, contains 176 000 tonnes of ore with an average ore grade of 4% Cu and 40.6% S (Çakır, 1995). Recently, Altun et al. (2015) reported huge additional ore reserves from Mağaradoruk deposit (up to 29 millions of tonnes) with average grades of 5.07%Cu, 0.56% Co, 2.10 g/t Au and 10.38 g/t Ag.

Current age constraints on the timing of mineralization comes from the deposit hosting stratigraphy. It has been suggested that the formation of the Küre VMS deposit is pre-Middle Jurassic (Kovenko, 1944; Güner, 1980). Based on their Rb-Sr and K-Ar radiometric ages, Terzioğlu et al. (2000) suggested existence of at least two different types of basalts in the Küre Complex, both in origin and in age (Bajocian; 170±6 Ma, 168±5 Ma and Berriasian-Valanginian; 137±3, 136±6 Ma; analytical media unspecified).These results were in good agreement with previous findings of CENTO group (Sarıcan, 1968) suggesting two major basaltic volcanic pulses clearly separated in time (cf. Güner, 1980). However, Kozur et al. (2000), on basis of stratigraphic relationships, noted that the mafic volcanic rocks in the Küre Complex should be older than Late Triassic (possibly middle Triassic). They disagreed with the Bajocian ages due to the low potassium contents of basalts and possible hydrothermal alteration effects and regarded the much younger Berriasian-Valanginian aged basalts as products of a later extensional process. Çakır et al. (2006) similarly suggested a careful approach to these data due to the probable low-temperature alteration effects, although noting that these are also supported by the paleontological data of Önder et al. (1987). The age interval pronounced for the black shale-subgraywacke ranges from Lower Permian to early Jurassic (cf. Koç et al., 1995; early Jurassic - Ketin, 1962; Yılmaz, 1979,1980; Permian - Güner, 1980; pre-early Jurassic - Pehlivanoğlu, 1985). However, correlations with the surrounding strata and few fossil findings suggest a Late Triassic to Middle Jurassic interval (Kovenko, 1944; Ketin, 1962; Aydın et al., 1986, 1995; Önder et al., 1987), as the older Upper Carboniferous to Lower Permian palynomorphs reported earlier (Kutluk and Bozdoğan, 1981) are largely considered to be reworked material from older lithologies (Yılmaz and Şengör, 1985; Ustaömer and Robertson, 1994; Kozur et al., 2000; Çakır et al., 2006).

3. Sampling and Analytical Methods

A total of seventeen samples were collected from the Küre VMS deposits. Nine of these samples are taken from different levels of a deep drill hole (M-256), two of them are from outcrops and six of them are from drifts. A schematic summary of the sample locations, types, depths, and lithologies are given in Figure 5. Each sample group represents different segments of the deposit. The drill hole M-256 presents a very thick black-shale sequence due to the tilted and folded orientation of the strata. This sequence is followed by a relatively thin massive and stockwork sulfide mineralization presumably marking originally a thinning distal edge of a larger massive sulfide lens. The ore samples gathered from this drill hole are composites from 961.50 to 968.10 meters. The drift samples are from 645 to 710 m levels, whereas the outcrop samples are collected from the batters and berms in the Bakibaba pit.

Twelve pieces of ore samples were selected from the massive and the stockwork ore and mounted in 1 inch diameter epoxy plugs and grinded-polished for both reflected light microscopy and micro-analytical studies. Also, six doubly polished thin sections (27x46 cm and ca. 100–200 μm thick) were prepared for microthermometric studies. These samples were selected from the suitable stockwork networks where several stages of overprinting quartz and calcite are found as veinlet fillings. The samples collected for Re-Os geochronology are selected from the massive sulfide ore, the sulfide-rich parts of the stockwork and the overlying black shale-subgraywacke unit. Six pyrite-rich sulfide concentrates were prepared and analyzed from the massive and the stockwork ore. The selected sulfide ore samples from the massive sulfide lenses and the stockwork ore were crushed and sieved to obtain five different size fractions. This is done to help to free different sizes of pyrites from their surrounding interlocking media to ease the handpicking process. Approximately 2000 mg of mineral separates rich in pyrite is obtained by handpicking for each sample. Three 0.2-1 meters of fine-grained and unmineralized black shale cores were also selected from the M-256 drill hole for whole-rock Re-Os analysis. Although there are large black shale-subgraywacke outcrops in the area (see Figure 3), core samples from M-256 drill hole are selected for analysis in order to avoid effects of weathering and oxidation.

The wavelength-dispersive spectrometry (WDS) analyses on selected sulfide minerals were carried out by a Cameca SX-100 electron-probe micro-analyzer (EPMA) installed at the Department of Earth and Environmental Sciences, Ludwig-Maximilians-University of Munich (Germany). The accelerating voltage, the probe current and the beam spot size were set to 15 keV, 40 nA and <1 μm, respectively. Pure metals were used as standards for Cu, Se, Te, Cd, Co, Ag, Au and Bi, whereas the rest of the standards were sphalerite for Zn and S, GaAs for As, Sb_2S_3 for Sb, and PbS for Pb. The X-ray lines used in the analyses are Lα for As, Se, Sb, Te, Cd and Ag, Kα for S, Fe, Ni, Zn, Co and Cu, and Mα for Au, Pb and Bi.

Microthermometric studies were carried out at the Fluid Inclusion and Ore Microscopy-Petrography Laboratory in the Department of Geological Engineering, Dokuz Eylul University (İzmir, Turkey). The studies were performed by a Linkam THMGS-600 heating-freezing stage mounted on a binocular Leica DMLP microscope with a maximum magnification of 1000X. The system is equipped with a Linkam TMS94 temperature controller and LNP94/2 liquid nitrogen pump. The temperature range of the stage used was −196°C to +600°C with a temperature stability and accuracy of ±0.1°C. Stage calibration was controlled by a set of standard resistances (for known temperatures values of -196.5, -44.5, 0.0, 117.2, 557.7 and 336.7 °C) provided by the Linkam Scientific Instruments Limited.

Six pyrite and two black shale samples were analyzed for their Re-Os abundances and isotope compositions. The analyses were performed at the Laboratory for Sulfide and Source Rock Geochronology and Geochemistry at the Durham Geochemistry Centre at Durham University, UK. The analytical protocols used follow those outlined by Selby et al. (2009; pyrite), and Selby and Creaser (2003), and Cumming et al. (2013; shale). In brief, ~50 mg of pyrite and ~1 g of black shale were loaded into a carius tube with a known amount of a tracer solution comprising ^{190}Os and ^{185}Re. For the pyrite samples 3 mL of 11N HCl and 6 mL of 15N HNO_3 was added to the carius tube. For the black shales samples 8 mL of 0.25 g/g CrO_3 in 4N H_2SO_4 was added to the carius tube. The carius tubes were sealed and placed in an oven at 220˚C for 48 hours. For both pyrite and black shale samples Os was isolated and purified from the acid medium using solvent extraction ($CHCl_3$) and micro-distillation methods. For the pyrite samples the Re fraction was isolated using anion chromatography. The Re fraction for the black shale samples was isolated using a 5N NaOH:Acetone solvent extraction followed by anion chromatography. Isotopic measurements were performed using a ThermoScientific TRITON mass spectrometer with static Faraday collection for Re and ion-counting using a secondary electron multiplier in peak-hopping mode for Os. Total procedural blanks for pyrite analysis are 3.0 ± 0.2 pg Re and 0.10 ± 0.02 pg Os (1 SD, n = 2), with an average $^{187}Os/^{188}Os$ 0.25 ± 0.02. For the black shale analysis the procedural blanks are 14 ± 1 pg Re and 0.50 ± 0.1 pg Os (n = 1), with $^{187}Os/^{188}Os$ 0.25 ± 0.10. In-house Re ($^{185}Re/^{187}Re$ = 0.5983 ± 0.001; n = 2) and Os (DROsS, $^{187}Os/^{188}Os$ = 0.16094 ± 0.003; n = 2) solutions run during the course of this study are both identical, and within uncertainty, to those previously reported (Du Vivier et al., 2014 and the references therein).

4. Results and Discussion

4.1. Sample Paragenesis and Ore Textures

As the main focus of this study is the Re-Os geochronology from the LLHR sulfides of the Küre VMS deposit, it is important to understand the paragenetic sequence and succession in the samples studied. Thus, we have completed detailed ore microscopic studies from the samples of the drill hole M-256 and the drifts. Çağatay et al. (1980), whom studied ore samples from both the Bakibaba and Aşıköy deposits, interpreted that the ore paragenesis, textures and structures of both mineralizations are similar and present a mineral paragenesis rich in primary sulfides, minor oxide phases as well as secondary sulfides, oxides and carbonates. The sample paragenesis we observed in our samples is similar to the previous work (e.g., Çağatay et al., 1980; Altun et al., 2015) with minor differences.

The samples investigated in this study are mainly dominated by pyrite and chalcopyrite that are accompanied by other sulfides, oxides and native metals. The massive ore samples are almost free of gangue phases, whilst the stockwork ore samples include veinlets of mainly quartz and calcite with accompanying opaque phases. Three distinct stages/processes are observable from the samples investigated. Chromite, anatase, hematite (Hm) and magnetite (Mgt) comprise the accessory pre-mineralization opaque phases in the basaltic host rocks. The ore assemblage is dominated by pyrite (Py) in all ore types, which is accompanied by subordinate chalcopyrite (CcpI and CcpII), sphalerite (SphI and SphII), cobaltite (Co), bravoite (Brv), marcasite (Mrc), melnikovite-pyrite (Mel-Py), bornite (Bo), hematite (Hm) and native gold (Au). Quartz (Qz) and calcite (Cal) are abundant in stockwork ore whereas chlorite (Chl) is found in basalts as an alteration mineral after ferromagnesian silicates. Deformation and recrystallization textures are attributed to post-mineralization folding, shearing, regional metamorphism and ophiolite obduction.

The pre-mineralization accessory opaque phase magnetite is partially and/or totally replaced by hematite (Fig. 6a). The hematite also shows flaky anhedral or needle-like/acicular forms and is occasionally found in the quartz veinlets and/or in the euhedral pyrite grains of the stockwork ore as small clots and inclusions (Fig. 6b). Pyrite is the oldest and the most dominant phase of both the massive and the stockwork ore. In the massive ore, pyrite (Py) is crystallized as euhedral, subhedral and anhedral aggregates ranging in size of hundreds of micrometers to millimeters (Fig. 6c). Pyrite grains are porous, relatively zoned and cataclastic, associated with the brittle deformation. Although chalcopyrite is by far the second most abundant sulfide in both ore types, it is more abundant in the massive ore than in the stockwork ore. The pyrites are embedded in a chalcopyrite dominated matrix (CcpI; Fig. 6c) and replaced by chalcopyrite and other sulfides along their edges and fractures. As reported by Kuşçu and Erler (2002), it appears that some fracture-filling chalcopyrite were formed as a result of remobilization during late-stage deformation. Sphalerite can be divided into two generations as SphI and SphII; the former showing intergrowths of chalcopyrite (CcpII) also known as “chalcopyrite disease”, and the latter being free of chalcopyrite (Figs. 6d, e and f). Bornite is present in trace amounts in massive ore. Where it is present, intergrowths of bornite with chalcopyrite exhibit complex exsolution textures (CcpII; Figs. 6f and g). The pyrites are also usually found interlocked with mostly euhedral/subhedral cobaltite grains (Co; Fig. 6h). In these pyrites, linear zones of bravoite (Brv; Fig. 6h) seperates the individul layers of pyrite.

Melnicovite-pyrite partially replaces pyrite (Py) and chalcopyrite (CcpI) and is replaced by pyrite, cobaltite and marcasite (Figs. 7a, b and c). Native gold is mainly found at the borders of pyrite and chalcopyrite (CcpI) and as minute inclusions in pyrite (Figs. 7d, e and f).

4.2. Compositions of the Main Sulfide Phases

Selected compositional data from the main ore phases (pyrite, chalcopyrite and sphalerite) are given in Table 1. Pyrite contains average values of 53.23 wt % S and 46.71 wt % Fe (n = 45). The pyrites correspond to the calculated structural formula $(Fe_{0.97-1.03}Cu_{0.00-0.02}Zn_{0.00-0.01}Co_{0.00-0.03})(As_{0.00-0.01}S_{1.97-2.00})$. The micro-chemical data also shows elevated contents of Co, Ag, Au and As in some of the pyrites. The Co content reaches up to 1.39 wt % (0.38 wt % on avg.), while the Ag and Au contents in pyrites reaches 0.09 and 0.11 wt % (0.08 and 0.11 wt % on avg.), respectively. Up to 0.57 wt % of As (avg. 0.16 wt %) is detected in pyrites. There is a significant negative correlation between Co and Fe (r = -0.565) and a significant positive correlation between Co and As (r = 0.625) showing substitution of Co for Fe and introduction of As in pyrite. Further Co-Fe exchange and As introduction is also visually traceable with the existence of cobaltite (CoAsS) intergrowths within pyrite (Fig. 6h).

The chalcopyrites include 34.70 wt % S, 30.24 wt % Fe and 33.57 wt % Cu on average (n=22). The calculated structural formula of chalcopyrite is $(Cu_{0.91-1.00}Fe_{0.99-1.03}Zn_{0.00-0.01})S_{1.99-2.05}$.

Sphalerites mainly comprise 33.10 wt % S, 60.42 wt % Zn and 3.41 wt % Fe in average (n = 5). The Cu contents in the sphalerite are also significantly high (1.16-3.77 wt%) leading to a calculated structural formula of $(Zn_{0.84-0.93}Fe_{0.04-0.10}Cu_{0.02-0.06})S_{1.00-1.02}$. Zn/Cd ratio of the sphalerite has been previously tested several times as an indicator for the genesis of the ore deposits (Jonasson and Sangster, 1978 ; Xuexin, 1984; Brill, 1989; Xu, 1998). The Cd content of the sphalerite mainly depends on the Cd/Zn ratio, ligand activities, and temperature of the ore forming fluids (Schwartz, 2000). The Zn/Cd ratios of the analyzed Küre VMS deposit sphalerites range in between 372 to 1417 with majority of the calculated ratios between 372 and 625 and an arithmetic average of 677. The sphalerite with the highest Zn/Cd ratio of 1417 presents a very low Cd content (0.04 wt %). This sphalerite is also richer in Fe (5.55 wt %) than the rest of the analyzed sphalerites (Fe contents between 2.41 to 3.5 wt %). The Zn/Cd ratios calculated from the sphalerites are presented in Figure 8 for comparison with the data from previous studies elsewhere and are in good agreement with the previous Zn/Cd data from volcano-sedimentary associations, volcanogenic massive sulfide deposits and their modern analogues. The ratios are also compare well with the whole-rock Zn/Cd ratios from basalts from elsewhere and partially correspond with mineralization systems including basaltic metal sources.

4.3. Fluid Inclusions Petrography and Microthermometry

The basaltic pillow lava host presents extensive chlorite alteration including fine-grained opaque phases. The quartz and calcite bearing veinlets comprising the stockwork ore in the chloritized host shows multiple episodes of hydrothermal fluid input with overlapping and overprinting quartz and calcite occurrences. We have determined two main episodes of fluid input from the stockwork ore samples that is interpreted by differing and overprinting/cross-cutting quartz occurrences and opaque mineral precipitation. The early quartz veinlets are >500 μm in thickness, and are cross-cut by thinner late-stage veinlets (Fig. 9a; Qz1 and Qz2 veinlets, respectively). The early-stage veinlets are also divided into two quartz occurrences overprinting each other (Fig. 9b; 1a and 1b, respectively). The former quartz occurrences (1a) in the early stage Qz1 veinlets include larger (>300 μm) and zoned quartz grains and limited opaque phases such as hematite (Figs. 9c and d). The latter quartz phase in the Qz1 veinlets (1b) comprise finer (microcrystalline) quartz grains and introduction of more extensive opaque phases representing the sulfide mineralization in the stockwork ore. The thinner Qz2 veinlets cross-cutting/overlapping the Qz1 veinlets also include sulfide mineralization (Fig. 9a). Calcite seems to be the latest phase in the stockwork veinlets as it crosscuts the former quartz occurrences and the ore minerals (Fig. 4d).

Microthermometric measurements are performed on fluid inclusions from quartz dominated stockwork ore obtained from the core samples of drill hole M-256 in the interval between 962 and 968 m above sea level. The fluid inclusions in the quartz veinlets of the stockwork (either Qz1 or Qz2) are scarce, extremely small and it is not possible to do microthermometric studies in most of the inclusions. The acquired microthermometric results from available fluid inclusions are given in Table 2. Inclusions from the quartz samples of stockwork ore are generally irregular-shaped inclusions and typically range in length from 5 to 20 μm. Petrographic examination of the thin section shows two-phase inclusions in quartz with vapor/liquid ratios between 4 to 28%. We have not observed any diagnostic features related to the secondary fluid inclusion formation. Due to the small sizes and scarcity of the fluid inclusions, it is also not possible to group and correlate fluid inclusions according to their quartz host phases (e.g., Qz1 and Qz2). However, two populations of fluid inclusions are determined solely on the base of homogenization temperatures versus salinity diagram (Fig. 10). The vapor bubbles from first population are variable in size and occupies about 20% of the inclusion volume (up to 30%). Fluid inclusions from first population homogenize to the liquid phase between 270.9°C and 317.0°C, with a mean of 289.9°C (Fig. 10). The final melting of the ice occurred with a final temperature range of -3 to -0.5°C which yielded salinities between 5.0 and 0.9% wt NaCl equiv. In second population, total homogenization into the vapor phase has been observed between 161.5 and 245.7°C with an average of 202.6°C. These inclusions showed final ice-melting temperatures varying between−2.4°C and

−1.2 °C which indicates salinities from 4.0 to 2.1% wt NaCl equiv. The average first melting temperatures (T_{mf}) of first and second population are at −48.2 °C and −37.2 °C, indicating a H_2O-$CaCl_2$-KCl-$MgCl_2$ ore-forming hydrothermal fluid system (Goldstein and Reynolds, 1994; Shepherd et al., 1985).

4.4. Re-Os Isotopes

The Re and Os concentrations and isotope compositions of the six separated pyrite-rich concentrates and two black shale samples are given in Table 3. The Re concentrations of the sulfides range between 132.9 to 630.9 ppb and total Os values range between 250.6 to 1175.2 ppt. In comparison, the black shale samples possess very low Re contents (0.63 and 1.15 ppb) and low Os (157.5-195.5 ppt) concentrations. The sulfide $^{187}Re/^{188}Os$ and $^{187}Os/^{188}Os$ ratios show wide ranges from 44545.1 to 329370.4 and 126.1 to 1614.1, respectively. The $^{187}Re/^{188}Os$ ratios for the black shales are 20.1 and 29.9 and the $^{187}Os/^{188}Os$ ratios obtained are 0.5171 and 0.5402. All sulfide samples have large $^{187}Re/^{188}Os$ and highly radiogenic $^{187}Os/^{188}Os$ ratios indicating the bulk of the ^{187}Os in the sample is radiogenic (Table 3). The Re and Os data of the sulfide concentrates indicate that the sulfides had minimal common Os at the time of formation. As a result, the initial $^{187}Os/^{188}Os$ value cannot be determined to investigate the source of Os and by inference the ore metals. In addition to the samples possessing $^{187}Re/^{188}Os$ values much greater than 5000 and highly radiogenic $^{187}Os/^{188}Os$ resulting in highly correlated uncertainties between the isotope ratios (rho; Table 3), two of the sulfide samples present widely different $^{187}Re/^{188}Os$ and $^{187}Os/^{188}Os$ values. As such no geological age using a traditional plot of $^{187}Re/^{188}Os$ *vs.* $^{187}Os/^{188}Os$ could be determined from the Re-Os data for all six samples (Fig. 11a).

The Re-Os data for the sulfide samples have features consistent with the low level highly radiogenic sulfides (LLHR; Stein et al., 2000). For such samples it is suggested that the

Re-Os isochron age should be determined in ^{187}Re-^{187}Os^{r} (radiogenic ^{187}Os) space to avoid uncertainties from the very low and difficult determinations of ^{188}Os (Stein et al., 2000; Selby et al., 2009; Nozaki et al., 2010). The ^{187}Os^{r} abundance (Table 3) was achieved using the initial ^{187}Os/^{188}Os value calculated from using four of the six samples that display a positive correlative between ^{187}Re/^{188}Os *vs.* ^{187}Os/^{188}Os (Fig. 11b). The regression of the Re-Os data for the four samples yield an age of 176 ± 22 Ma (initial ^{187}Os/^{188}Os = -6 ± 37; MSWD = 11.2). A ^{187}Re-^{187}Os^{r} plot of Küre sulfides yields the same age, with uncertainty, as the traditional Re-Os plot (175 ± 19 Ma), but with significantly less scatter (MSWD = 0.23, Fig. 11c). The ^{187}Re-^{187}Os^{r} plot also indicates the near absence of common ^{187}Os (initial ^{187}Os^{r}, 2 ± 68 ppt). Additionally the ^{187}Re and ^{187}Os^{r} data permit model ages to be determined. Model ages for the four samples are nominally different, but identical within uncertainty (Table 3). A weighted average of the model ages is 176 ± 11 Ma (6.1%, with a confidence level of 95%; MSWD = 0.16; Fig. 11d). All of these Re-Os data suggests a nominal age of upper Toarcian (uppermost early Jurassic). The remaining two discordant samples (BK-US and M256/V1) present largely different model ages (320.8 ± 37.4 and 138.2 ± 7.2 Ma, respectively; Table 3). The older model age is from an outcrop sample with disseminated ore and the younger one is from a stockwork sample from the drill hole.

Two samples selected and analyzed from the black shale-subgraywacke strata, overlying the massive sulfide lens, possess low Re values and are not useful for geochronological constraints. However, the data may facilitate to make a preliminary approach to the initial Os isotope ratio [^{187}Os/^{188}Os$_{(i)}$] of the contemporaneous seawater, as the chemical and isotopic compositions of marine sediments/precipitates are expected to reflect the conditions of the seawater in which they had been accumulated (e.g., Cohen et al., 1999). The initial Os isotope ratios of the black shale samples at 180 Ma are 0.45 and 0.46.

4.5. Age of the Sulfide Mineralization and Implications

The late Paleozoic to early Mesozoic paleogeographic history of the Tethyan realm in northern Turkey is an important topic of debate. Within this debate, the geodynamic setting and geological history of the Sakarya Terrane that include the Küre and the Karakaya Complexes is extensively discussed in the literature (cf. Göncüoğlu, 2010 and the references therein; Fig. 12a). In summary, the Sakarya Terrane is assumed to have rifted from Gondwana and accreted to Eurasia during the Late Palaeozoic (Robertson and Ustaömer, 2009). In this context, the Karakaya Complex is believed to represent a Permo-Triassic accretionary complex sliced with other Late Paleozoic-Triassic accretionary complexes of the Paleotethyan active margin (Göncüoğlu, 2010). The Mid-Triassic-Mid Jurassic Küre Complex on the other hand, is also correlated with the Karakaya Complex and is generally regarded as a back arc basin that has opened behind the volcanic arc (e.g., Robertson and Ustaömer, 2009).

Previous researchers has provided various paleogeographic models and reconstructions of the region. These models regard the Küre ophiolitic complex as a remnant of a subduction zone, mainly conflicting on either the interpretation of the subduction direction or the setting of the contemporaneous Küre and Karakaya basins. In one of the models, the Küre Complex is described as the remnant of the southward subducting Late-Paleozoic-Triassic Paleo-Tethys, proposing that the units of the Karakaya complex originated from a rift-related narrow oceanic marginal basin (Bingöl et al., 1975, Şengör, 1979, Şengör and Yılmaz, 1981; Şengör, 1984; 1985; Şengör et al, 1980a,b; Şengör et al, 1984; Yılmaz et al, 1994 a, b.; Okay and Mostler, 1994; Genç and Yılmaz, 1995; Yılmaz et al., 1997; Yiğitbaş et al, 1999; Kozur et al., 2000). In a second model, the Karakaya Basin is contrastingly interpreted as the remnant of the Paleo-Tethys, and the Küre Basin as the small back-arc basin that opened by the northward subduction of the Karakaya oceanic lithosphere (e.g., Pickett et al., 1995; Pickett and Robertson, 1996; Ustaömer and Robertson, 1994; 1995; 1997; 1999;

Okay et al., 1996; Kozur et al., 2000). According to Şengör and Yılmaz (1981) opening and closure of Karakaya Ocean is restricted in the Triassic. The advocates of the second model asserted that Küre back-arc basin was opened during Permian to early Jurassic by the northward subduction of the oceanic lithosphere of the Karakaya Ocean, which is regarded as a large long-lived (Devonian to Triassic) Paleo-Tethyan ocean (cf. Ustaömer and Robertson, 1994; Kozur et al., 2000 and references therein). A third model (Okay and Tüysüz, 1999; Okay, 2000) disparately considers both oceanic basins as relics of the same single large Paleo-Tethys and suggests that they have separated with later events (Kozur et al., 2000). The Karakaya complex is interpreted as a subduction-accretion complex, which is being formed by the northward subduction of Karakaya oceanic lithosphere beneath Laurasia by Okay (2000). Kozur et al. (2000), arguing on the grounds of the fossil and stratigraphic data, suggest that none of the assumptions and suggestions in all these three models are fully correct. These authors remark that: (1) the Karakaya Basin is a latest Permian-Upper Triassic oceanic rift basin, (2) the Küre Basin is a Lower Triassic-Middle Jurassic southward subducting back-arc basin, and (3) no field data is available on the northward subduction of a combined Karakaya-Küre Ocean (a single and huge Carboniferous-Middle Jurassic Paleo-Tethys). More recent, newer reconstructions for the region involve a multi-armed (Paleotethys, Küre, Meliata, Maliac, Pindos, etc) Late-Paleozoic-Triassic Tethys with an additional oceanic branch between the Taurides (s.s.) and the Anatolides with no clear consensus on the number, locations, life-spans and subduction polarities of these oceanic branches/marginal basins and the Karakaya Complex as a product of the closure (cf. Göncüoğlu, 2010 and the references therein; Fig. 12b).

The Re-Os isotopic study of the LLHR sulfides from the Küre VMS Deposit has given a nominal age of upper Toarcian (uppermost early Jurassic) for sulfide mineralization. Both the Küre Complex and the Küre VMS deposit were previously interpreted to be subjected at least to regional greenschist facies conditions during/after their emplacement/accretion (e.g., Aydın et al., 1986; Kuşçu and Erler, 2002), and metamorphic processes are known to disturb the Re-Os systematics, especially for minerals such as sphalerite and pyrrhotite (e.g., Morelli et al., 2004, 2010; Nozaki et al., 2013). However pyrite and chalcopyrite from samples that underwent greenschist facies metamorphism, can yield reliable Re-Os ages preserving the primary Re-Os isotope composition from the time of its formation (Brenan et al., 2000; Selby et al., 2009; Nozaki et al., 2013). Given that all of the sulfides analyzed for the Re-Os isotopes in this study are from the handpicked separates of pyrite-chalcopyrite dominated sulfide mineralization, we interpret these results to represent original depositional ages. Although, we cannot totally rule out minor (e.g., overlooked) presence of any other sulfides that may slightly disturb the Re-Os isotope system, both isochron plots in the ^{187}Re/^{188}Os *vs.* ^{187}Os/^{188}Os and the ^{187}Re-^{187}Os^{r} space yield very similar ages within their uncertainties, and are interpreted to represent the depositional age of sulfide mineralization. The results are also in agreement with the previous field based pre-Middle Jurassic interpretation of Kovenko (1944), and the Permian-early Jurassic age interval pronounced for the lifespan of Küre back-arc basin (e.g., Ustaömer and Robertson, 1994).

In light of the likely primary upper Toarcian age for the mineralization, the simplest inference is the continuation of the extensional regime in the Küre Basin during setting of the VMS deposition. However, the Re-Os geochronological data also supports the second paleogeographic model discussed above (e.g., Pickett et al., 1995; Pickett and Robertson, 1996; Ustaömer and Robertson, 1994; 1995; 1997; 1999; Okay et al., 1996), which interpreted the Küre Basin as a back-arc marginal basin of a northward subducting Karakaya Ocean; this appears to be the more likely model for the setting of the Küre VMS deposit. Data from an outcrop sample and a drilled stockwork sample with largely different model ages that are rejected from the isochron plots (BK-US; 320.8 ± 37.4 and M256/V1; 138.2 ± 7.2 Ma, respectively) may be affiliated with some other pyrite crystallization events prior to and postdating the main sulfide deposition. Unfortunately, our data does not allow us to make a correlation between the ages and the chemical compositions of the pyrites. Hence, we prefer to avoid commenting on the nature of the older model age of the outcrop sample. However, the younger pyrite age from the stockwork may be questioned in relation to the fluid inclusions microthermometry from the quartz veinlets of the stockwork.

In volcanogenic massive sulfide (VMS) systems, physicochemical characteristics of fluid inclusions depend on PVTX conditions of the location where the fluid inclusions are trapped within the hydrothermal system. In VMS environment, the characteristics of the fluid inclusions can vary systematically from location to location and even within the same paragenesis and the fluid inclusion temperatures in VMS stockworks are typically in the range 200-400°C (Hannington et al., 1998; Lüders et al., 2001). Above the two-phase zone, along the rising plume, fluid inclusions are liquid-rich with salinity slightly higher than or lower than that of seawater, and have homogenization temperatures between 200 and 400°C (Steele-MacInnis et al., 2012). In Küre, the fluid inclusions of quartz from the stockwork zone are two-phase inclusions. Most of the measured homogenization temperatures fall in between 200-300 °C (n=17). The inclusions are liquid-rich and contain vapor bubbles occupying about up to 30 volume percent of the inclusion. The lack of coexisting vapor-rich and halite-bearing inclusions indicates ore formation in shallower subsurface near the seafloor vents (up to 0.5 km in depth) where the inclusions are liquid-rich. The low salinities reflect mixing between sea water and phase separated brine and/or vapor from the deeper part of the system. The similarity of fluid salinity to normal seawater (3.5 wt % NaCl equiv) further suggests the input of a large amount of cold seawater into the Küre hydrothermal system. These data show that the bulk of the microthermometric data is in good agreement with the above given literature. However, lower homogenization temperatures below 200 °C (n=4) and the younger pyrite age from the stockwork may still suggest that at least some of the stockwork veinlets in the deposit are younger and are related to the post-VMS deformation/mineralization events.

The new depositional age data partially contradicts with previous arguments of Kozur et al. (2000) that suggest older than Late Triassic (possibly middle Triassic) age for the mafic volcanic rocks of the Küre Complex. However, we must note that the new isotopic data we present gives the direct age of deposition for the Küre VMS Deposit, and may also imply an upper age limit for the basaltic volcanism (Fig. 12c). We may suggest that a submarine volcanic extrusion episode continued up to upper Toarcian, reaching a period of stagnation, allowing a continuous and long-term seawater circulation and hydrothermal fluid discharge for the formation of the Küre sulfide mounds. The Middle Jurassic ages obtained from the basalts (Bajocian; 170±6 Ma and 168±5 Ma; Terzioğlu et al., 2000) are also in good agreement with the Re-Os isotopic ages obtained in this study within errors. It appears with the current data that the beginning of the closure of the Küre Basin had not been initiated before the uppermost early Jurassic. Hence, the early Cretaceous (Berriasian-Valanginian: 137±3, 136±6 Ma) ages by Terzioğlu et al. (2000) present a different late episode of volcanic activity, as indicated by previous researchers (e.g., Sarıcan, 1968; Güner, 1980; Terzioğlu et al. 2000; Kozur et al., 2000).

We were unable to constrain the depositional age of the black shale-subgraywacke strata of the hemipelagic muds and terrigenous turbidites that are interpreted to blanket the Küre ocean basin following volcanic and hydrothermal activity (e.g., Ustaömer and Robertson, 1994). However, the depositional age for the siliciclastic sediments of the Küre Complex has been previously reported to span mainly in a Late Triassic to Middle Jurassic interval (Kovenko, 1944; Ketin, 1962; Aydın et al., 1986, 1995; Önder et al., 1987). Kozur et al. (2000) managed to further confine the age of the lower and middle segments of the siliciclastic sediments from middle Carnian to middle Norian interval (Late Triassic). They also noted that the age interval of the upper segment should be between middle Norian and Late Jurassic. Hence, the proposed depositional age range of the siliciclastic sediments and the seafloor volcanism prior to the deposition of the sulfides seem to partially overlap (Fig. 12c). This is in good agreement with the previously presented lithological evidences on contemporaneous deposition of the lower segment of the organic-matter rich sediments and the upper segment of the basaltic volcanic rocks (e.g., Tüysüz, 1986; Pehlivanoğlu, 1985; Çakır, 1995) and again may support a stagnation period in the submarine volcanic extrusion during the upper Toarcian.

The $^{187}Os/^{188}Os$ ratios of the sulfide samples are highly radiogenic and do not to allow us to propose a source for Os. On the other hand, the large variations in the initial Os isotope ratios [$^{187}Os/^{188}Os_{(i)}$] of seawater are usually attributed to inputs by continental, mantle (volcanic and hydrothermal), and cosmogenic events, the former one resulting in very radiogenic (1.0-1.5; Peucker-Ehrenbrink and Jahn, 2001) and the latter two concluding in very unradiogenic Os isotopic ratios (e.g., 0.12-0.13; Allègre and Luck, 1980) (Tejada et al., 2009). The very limited $^{187}Os/^{188}Os_{(i)}$ data (0.45 and 0.46, calculated for 180 Ma) from two black shale samples blanketing the Küre VMS deposit are in agreement with the wide $^{187}Os/^{188}Os_{(i)}$ interval of the Early Jurassic seawater (from ~0.4 to ~1.0; Cohen et al., 2004), coinciding with the lower limit range. However, the available data is statistically inadequate to make a significant deduction. Hence, the reply to this question currently stays unresolved. More data from the black shale strata is needed to constraint the Os isotopic composition of the contemporaneous seawater and the source(s) of Os in the depositional environment of the Küre VMS deposit.

5. Conclusions

This study presents new paragenetic, compositional, microthermometric and geochronological datasets from the Küre VMS deposit located in Central Pontide region, northern Turkey. The massive and stockwork ore selected for the dating studies were pyrite-dominant with subordinate chalcopyrite, sphalerite and other sulfide species. Stockwork ore included quartz and calcite gangue veinlets, while the massive ore is almost free of gangues. Mineral chemistry of the sphalerites show typical ranges described for the ancient volcanogenic massive sulfide deposits/mineralizations and their modern analogues elsewhere. Microthermometric data provided from the quartz gangue of the stockwork ore showed low to intermediate homogenization temperatures (T_h) and low salinities, also being mostly in good agreement to the ranges encountered in volcanogenic massive sulfide mineralizations. The average first melting temperatures (T_{mf}) obtained from the microthermometry pointed out a H_2O-$CaCl_2$-KCl-$MgCl_2$ ore-forming hydrothermal fluid system. The salinity data (slightly greater or less than that of seawater) obtained from the two-phase inclusions and the lack of coexisting vapor-rich and halite-bearing inclusions are used to constraint a depth for the sampled stockwork ore formation, which is presumably at a shallower subsurface environment near the seafloor vents (up to 0.5 km in depth).

This first attempt of Re-Os dating of the LLHR sulfides from the Küre VMS Deposit yield a nominal age of upper Toarcian (uppermost early Jurassic) for this well-known Cyprus-type massive sulfide mineralization located in the Central Pontides in northern Turkey. The studies are conducted on handpicked pyrite concentrates obtained from the crushed sulfide ore fractions to minimize effects of regional metamorphism on the mineralization. No geological age could be determined from the Re-Os data for all six samples using a traditional plot of $^{187}Re/^{188}Os$ *vs.* $^{187}Os/^{188}Os$. However, four of the six sulfide samples displayed a positive correlation between $^{187}Re/^{188}Os$ *vs.* $^{187}Os/^{188}Os$ and yielded an age of 176 ± 22 Ma. The Re-Os isochron age is also determined in ^{187}Re-^{187}Os^{r} (radiogenic^{187}Os) space and yield the same age, with uncertainty, as the traditional Re-Os plot (175 ± 19 Ma). Thus, the upper Toarcian age is considered to present the timing of the main sulfide deposition. Two largely different model ages in two of sulfide samples (320.8 ± 37.4 and 138.2 ± 7.2 Ma) are attributed to some other pyrite crystallization events prior to and postdating the main sulfide deposition. Some lower homogenization temperatures from the quartz of the stockwork (<200°C, n=4) may also be correlated to the post-VMS events. The upper Toarcian depositional age of the Küre VMS deposit implies that the ongoing submarine volcanic extrusion episode in the Küre basin has presumably entered a stagnation stage during upper Toarcian allowing the hydrothermal circulation and discharge of the sulfide-laden fluids to the ocean floor. Hence, the data also support the paleotectonic models that interpret the Küre Ocenic Basin as a Permian-early Jurassic back-arc basin of a northward subducting Devonian to Triassic Karakaya Ocean.

The lack of common Os from the sulfides does not let us to infer a source of Os form this data. Still, the limited Re-Os isotopic knowledge obtained from the black-shale strata blanketing the mineralization provides us an idea on the initial ^{187}Os/^{188}Os ratio of contemporaneous sea water (0.45-0.46 for 180 Ma). A further detailed study focusing on the isotopic composition of the black shale strata may help to constrain the Os isotopic composition of the contemporaneous seawater and the source(s) of Os in the depositional environment of the Küre VMS deposit.

Acknowledgements

The authors would like to thank Eti Bakır Joint-Stock Corporation and company officials Dr. Yılmaz Altun, Hüseyin Yılmaz, İlyas Şiner and Fatih Yazar for their assistance during the field and sampling studies. The authors are also grateful to the anonymous reviewer and Dr. Stephen J. Piercey for their constructive comments on the earlier version of the manuscript. This study is funded by the Dokuz Eylül University Scientific Research Project 2012.KB.FEN. 048.

References

Alişan, C., Aköz, Ö., Kırıcı, S., 1992. Kastamonu, Küre, Azdavay yöresi 1990 Yılı Saha Çalışmalarına Örneklerin Palinoloji, Nannoplankton ve Mikropaleontoloji Analizleri.- Turkish Petroleum Corporation, Exploration Group, Report no. 2965, Ankara (unpublished).

Allègre C-J, Luck JM. 1980. Osmium isotopes as petrogenetic and geological tracers. Earth and Planetary Science Letters 48, 148–154.

Altun, Y., Yılmazi H., Şiner, İ., Yazar, F., 2015. Okyanus ortası sırtlarda oluşan masif sülfid yataklarının sırları ve Küre-Mağaradoruk bakır yatağı. Bulletin of the Mineral Research and Exploration 150, 51-65.

Arne, D.C., Bierlein, F.P., Morgan, J.W., Stein, H.J., 2001. Re-Os dating of sulfides associated with gold mineralization in Central Victoria, Australia. Economic Geology 96, 1455-1459.

Aydın, M., Şahintürk, O., Serdar, H.S., Özçelik, Y., Akarsu, İ., Üngör, A., Çokuğraş, R., Kasar, S., 1986. Ballıdağ-Çangaldağı (Kastamonu) arasındaki bölgenin jeolojisi. Bulletin of Geological Society of Turkey 29, 1-16.

Aydın, M., Demir, O., Özçelik, Y., Terzioğlu, N., Satır, M., 1995. A geological revision of İnebolu, Devrekani, Ağlı and Küre areas: new observations in Paleotethys-Neotethys sedimentary succession, in: Erler, A., Ercan, T., Bingöl, E., Örçen, S. (Eds.), Proceedings of the International Symposium on the Geology of the Black Sea Region. Mineral Research and Exploration Institute of Turkey (MTA) Publications, Ankara, pp. 33–44.

Bailey, E.H., Barnes, J.W., Kupfer, D.H., 1966. Geology and Ore Deposit of the Küre District, Kastamonu Province, Turkey, in: CENTO Summer Training Program in Geological Mapping Techniques, pp. 17-73.

Barrie, C.T., Hannington, M.D., 1999. Introduction: Classification of VMS deposits based on host rock composition, in: Barrie, C.T., and Hannington, M.D. (Eds.), Volcanic Associated Massive Sulfide Deposits: Processes and Examples in Modern and Ancient Settings. Reviews in Economic Geology, v. 8, pp. 2-10.

Bingöl, E., Akyürek, B., Korkmazer, B., 1975. Biga yarımadasının jeolojisi ve Karakaya formasyonunun bazı özellikleri. Cumhuriyetin 50. Yılı Yerbilimleri Kongresi Tebliğleri, Mineral Research and Exploration Institute of Turkey (MTA) Publications, 70-77.

Bischoff, J.L., Rosenbauer, R.J., Aruscavage, P.J., Baedecker, P.A., Crock, J.G., 1983. Sea-floor massive sulfide deposits from 21°N, East Pacific Rise, Juan de Fuca Ridge, and Galapagos Rift: bulk chemical composition and economic implications. Economic Geology 78, 1711–1720.

Boztuğ, D., Debon, F., Le Fort, P., Yılmaz, O., 1995. High compositional diversity of the Middle Jurassic Kastamonu plutonic belt, Northern Anatolia, Turkey. Turkish Journal of Earth Sciences 4, 67–86.

Brenan, J.M., Cherniak, D.J., Rose, La.A., 2000. Diffusion of osmium in pyrrhotite and pyrite: implications for closure of the Re-Os isotopic system. Earth and Planetary Science Letters 21, 19-27.

Brill, B.A., 1989. Trace-element contents and partitioning of elements in ore minerals from the CSA Cu-Pb-Zn deposit, Australia. The Canadian Mineralogist 27, 263-274.

Çağatay, A., Pehlivanoğlu, H., Altun Y., 1980. Küre piritli bakır yataklarının kobalt-altın rnineralleri ve yataklann bu metaller açısından ekonornik değeri. Bulletin of the Mineral Research and Exploration 93/94, 110-117.

Çakır, Ü., 1995. Geological characteristics of the Aşıköy-Toykondu (Küre-Kastamonu) massive sulfide deposits. Bulletin of the Mineral Research and Exploration 117, 29-40.

Çakır, Ü., Genç, Y., Paktunç, D., 2006. Intrusive lherzolites within the basalts of Küre ophiolite (Turkey): an occurrence in the Tethyan suprasubduction marginal basin. Geological Journal 41, 123-143.

Cohen, A.S., Coe, A.L., Bartlett, J.M., Hawkesworth, C.J., 1999. Precise Re-Os ages of organic rich mudrocks and the Os isotope composition of Jurassic seawater. Earth and Planetary Science Letters 167 (3-4), 159-173.

Cohen, A.S., Coe, A.L., Harding, S.M., Schwark, L., 2004. Osmium isotope evidence for the regulation of atmospheric CO_2 by continental weathering. Geology 32 (2), 157-160.

Creaser, R.A., Sannigrahi, P., Chacko, T., Selby, D., 2002. Further evaluation of the Re–Os geochronometer in organic-rich sedimentary rocks: a test of hydrocarbon maturation effects in the Exshaw formation, Western Canada Sedimentary Basin. Geochimica et Cosmochimica Acta 66, 3441-3452.

Cumming, V.M., Poulton, S.W., Rooney, A.D., Selby, D., 2013. Anoxia in the terrestrial environment during the late Mesoproterozoic. Geology 41, 583-586.

Demirbaş, T.T., Ağaoğlu, F., 1980. Küre-Aşıköy Cevher Yataklarının Gelişme Dönemleri ve Bugünkü Durumu Hakkında Rapor. Etibank Küre Bakırlı Pirit İşletmesi Müessesesi, 31p. (unpublished).

Du Vivier, A.D.C., Selby, D., Sageman, B.B, Jarvis, I., Gröcke, D.R. & Voigt, S. (2014). Marine $^{187}Os/^{188}Os$ isotope stratigraphy reveals the interaction of volcanism and ocean circulation during Oceanic Anoxic Event 2. Earth And Planetary Science Letters 389 (1), 23-33.

Erler, A., 1984. Tectonic setting of the massive sulfide deposits of the Southeast Anatolian Thrust Belt, in: Tekeli, O., Göncüoğlu, C. (Eds.), Geology of the Taurus Belt. M.T.A.-T.J.K. Yayını, pp. 309-316.

Fouquet, Y., von Stackelberg, U., Charlou, J.L., Erzinger, J., Herzig, P.M., Mühe, R., Wiedicke, M., 1993. Metallogenesis in Back-Arc Environments: the Lau Basin example. Economic Geology 88, 2154–2181.

Franklin, J.M., Lydon, J.W., and Sangster, D.F., 1981. Volcanic-associated massive sulfide deposits; in: Skinner, B.J. (Ed.), Economic Geology 75th Anniversary Volume: Society of Economic Geologists, pp. 485-627.

Franklin, J.M., Gibson, H.L., Jonasson, I.R., Galley, A.G., 2005. Volcanogenic Massive Sulfide Deposits, in: Hedenquist, J.W., Thompson, J.F.H., Goldfarb, R.J., Richards, J.P. (Eds.), Economic Geology 100th Anniversary Volume: The Economic Geology Publishing Company, pp. 523-560.

Fu X., Wang J., Qu W., Duan, T., Du, A.D., Wang, Z., Liu, H., 2008. Re-Os (ICP-MS) dating of marine oil shale in the Qiangtang basin , Northern Tibet , China. Oil Shale 25 (1), 47-55, doi:10.3176/oil.2008.1.06.

Galley, A.G., Hannington, M.D., and Jonasson, I.R., 2007. Volcanogenic massive sulphide deposits, in: Goodfellow, W.D. (Ed.), Mineral Deposits of Canada: A Synthesis of Major Deposit-Types, District Metallogeny, the Evolution of Geological Provinces, and Exploration Methods. Geological Association of Canada, Mineral Deposits Division, Special Publication No. 5, pp. 141-161.

Genç, Ş.Ç., Yılmaz, Y., 1995. Evolution of the Triassic continental margin, northwest Anatolia. Tectonophysics 243, 193-207.

Goldstein, R.H., Reynolds, T.J., 1994. Systematics of Fluid Inclusions in Diagenetic Minerals. SEPM (Society for Sedimentary Geology) Short Course 31, USA, 199p.

Goodfellow, W.D., Blaise, B., 1988. Sulphide formation and hydrothermal alteration of hemipelagic sediments in Middle Valley, Northern Juan de Fuca Ridge. The Canadian Mineralogist 26, 675–696.

Goodfellow, W.D., Franklin, J.M., 1993. Geology, mineralogy, and chemistry of sediment-hosted clastic massive sulfides in shallow cores, Middle Valley, Northern Juan de Fuca Ridge. Economic Geology 88, 2037–2068.

Gottesman W., Kampe, A., 2007. Zn/Cd ratios in calcsilicate-hosted sphalerite ores at Tumurtijn-ovoo, Mongolia. Chemie der Erde Geochemistry 67, 323-328.

Göncüoğlu, M.C., 2010. Introduction to the Geology of Turkey: Geodynamic Evolution of the Pre-Alpine and Alpine Terranes. General Directorate of Mineral Research and Exploration Monography Series 5, 69p.

Guo, W.M., Lu J.J., Jiang S.Y., Zhang, R.Q., Qi, L., 2011. Re-Os isotope dating of pyrite from the footwall mineralization zone of the Xinqiao deposit, Tongling, Anhui Province: Geochronological evidence for submarine exhalative sedimentation. Chinese Science Bulletin 56, 3860-3865, doi: 10.1007/s11434-011-4770-y.

Güner, M., 1980. Geology and massive sulfide ores of the Küre area, the Pontic Ranges, northern Turkey. Bulletin of the Mineral Research and Exploration 93/94, 65-109.

Hannah J. L., Bekker A., Stein H. J., Markey R. J., Holland H. D., 2004. Primitive Os and 2316 Ma age for marine shale: implications for Paleoproterozoic glacial events. Earth and Planetary Science Letters 225, 43–52.

Hannah, J.L., Stein, H.J., Yang, G., Zimmerman, A., Bingen, B., 2008. Re-Os dating of black shales: Timing and duration of sedimentary processes. AAPG Annual Convention Oral Presentations, Search and Discovery Article #40365 (2008), 45p.

Hannington, M.D., Galley, A.G., Herzig, P.M., Petersen, S., 1998. COmpariso of the TAG mound and stockwork complex with Cyprus-type massive sulfide deposits, in: Herzig, P.M., Humphris, S.E., Miller, D.J., Zierenberg, R.A. (Eds.), Proceedings of the Ocean Drilling Program Scientific Results Volume 158. Integrated Ocean Drilling Program, College Station TX USA, pp. 389-415.

Hannington, M.D., Scott, S.D., 1988. Mineralogy and geochemistry of a hydrothermal silica-sulfide-sulfate spire in the caldera of Axial Seamount, Juan de Fuca Ridge. The Canadian Mineralogist 26, 603–625.

Herzig, P.M., 1988. A mineralogical, geochemical and thermal profile through the Agrokipia "B" hydrothermal sulfide deposit, Troodos Ophiolith complex, Cyprus, in: Friedrich, G.H., Herzig, P.M. (Eds.), Base Metal Sulfide Deposits. Springer, Berlin, Heidelberg, pp. 182–215.

Hou, Z., Wang, S., Du, A., Qu, X., Sun, W., 2003. Re-Os dating of sulfides from volcanogenic massive sulfide deposit at Gacun, southwestern China. Resource Geology 53 (4), 305-310.

JICA and MMAJ 1992. The Republic of Turkey Report on the Mineral Exploration of Küre Area. Etibank Report: Ankara.

Jonasson, I.R., Sangster, D.F., 1978. Zn:Cd ratios for sphalerites separated from some Canadian sulphide ore samples, Paper Geol. Surv. Canada 78-1B, 195–201.

Kato Y., Suzuki K., Nakamura K., Hickman A. H., Nedachi M., Kusakabe M., Bevacqua D. C., Ohmoto H., 2009. Hematite formation by oxygenated groundwater more than 2.76 billion years ago. Earth and Planetary Science Letters 278, 40–49.

Kay, W., Hubbard, N., 1978. Trace elements in ocean ridge basalts. Earth and Planetary Science Letters. 38, 95–116.

Kendall, B., Creaser, R.A., Selby, D., 2006. Re-Os geochronology of post glacial black shales in Australia: constraints on the timing of "Sturtian" glaciation. Geology 34, 729-732.

Ketin, İ., 1962. 1:500 000 Ölçekli Jeolojik Harita ve İzahnamesi (Sinop): MTA yayınları, Ankara, Turkey.

Ketin, İ., Gümüş, Ö., 1963. Sinop, Ayancık ve Güneyinde, III. Bölgeye Dahil Sahaların Jeolojisi Hakkında Rapor I-II. Turkish Petroleum Corporation (TPAO) Report 213-218 (unpublished).

Kerr, A., Selby, D., 2010. The timing of gold mineralization on the Baie Verte Peninsula: Progress report on Re-Os pyrite geochronology. Current Research (2010) Newfoundland and Labrador Department of Natural Resources Geological Survey Report 10-1, 41-50.

Koç, Ş., Ünsal, A., Kadıoğlu, Y.K., 1995. Küre (Kastamonu) cevherleşmelerini içeren volkanitlerin jeolojisi, jeokimyası ve tektonik konumu. Bulletin of the Mineral Research and Exploration 117, 41-45.

Kovenko, V., 1944. Küre'deki eski bakır yatağı ile yeni keşfedilen Aşıköy yatağının ve Karadeniz orta ve doğu kesimleri sahil bölgesinin metallojenisi. Bulletin of the Mineral Research and Exploration 32, 180-212.

Kozur, H.W., Aydın, M., Demir, O., Yakar, H., Göncüoğlu, M.C., Kuru, F., 2000. New stratigraphic and palaeogeographic results from the Palaeozoic and Early Mesozoic of the Middle Pontides (northern Turkey) in the Azdavay, Devrekani, Küre and Inebolu areas: Implications for the Carboniferous-Early Cretaceous geodynamic evolution and some related remarks to the Karakaya Oceanic Rift Basin. Geologica Croatica 53(2), 209-268.

Kuşçu, İ., Erler, A., 2002. Pyrite deformation textures in the deposits of the Küre Mining District (Kastamonu-Turkey). Turkish Journal of Earth Sciences 11, 205-215.

Kutluk, H., Bozdoğan, N., 1981. Preliminary Repost of Palynology in the Sediments of Late Palaeozoic-Lower Mesozoic of the region IV. TPAO Report, Ankara (unpublished).

Large, R.R., 1992. Australian volcanic-hosted massive sulphide deposits: features, styles and genetic models. Economic Geology 87, 471-510.

Liu, Y.L.,Yang, G., Chen, J.F., Du, A.D., Xie, Z., 2004. Re-Os dating of pyrite from Giant Bayan Obo REE-Nb-Fe deposit. Chinese Science Bulletin 49, 2627–2631.

Lüders, V., Pracejus, B., Halbach, P., 2001. Fluid inclusion and sulfur isotopes studies in probable modern analogue Kuroko-type ores from the JADE hydrothermal field (central Okinawa Trough, Japan). Chemical Geology 173, 45-58.

Mathur R., Ruiz J., Tornos F., 1999. Age and sources of the ore at Tharsis and Rio Tinto, Iberian Pyrite Belt, from Re–Os isotopes. Mineralium Deposita 34, 790–793.

Misra, K.C., 2000. Understaning Mineral Deposits. Kluwer Academic Publishers, Dordrecht, Netherlands, 844p.

Morelli, R.M., Bell, C.C., Creaser, R. A., Simonetti, A., 2010. Constraints on the genesis of gold mineralization at the Homestake Gold Deposit, Black Hills, South Dakota from rhenium-osmium sulfide geochronology. Mineralium Deposita 45, 461–480.

Morelli, R.:, Creaser, R.A., Selby, D., Kelley, K.D., Leach, D.L., King, A.R., 2004. Re-Os sulfide geochronology of the Red Dog sediment-hosted Zn-Pb-Ag deposit, Brooks Range, Alaska. Economic Geology 99, 1569-1576.

Morelli R. M., Creaser R. A., Selby D., Kontak D. J., Horne R. J., 2005. Rhenium–osmium geochronology of arsenopyrite in Meguma Group gold deposits, Meguma Terrane, Nova Scotia, Canada: evidence for multiple gold-mineralizing events. Economic Geology 100, 1229–1242.

Nikitin, V., 1926. Küre Bakır Madeni. General Directorate of Mineral Research and Exploration (MTA) Report 850 (unpublished).

Nozaki, T., Kato, Y., Suzuki, K., 2010. Re-Os geochronology of the Iimori Besshi-type massive sulfide deposit in the Sanbagawa metamorphic belt, Japan. Geochimica et Cosmochimica Acta 74, 4322-4331.

Nozaki, T., Kato, Y., Suzuki, K., 2013. Late Jurassic ocean anoxic event: evidence from voluminous sulphide deposition and preservation in the Panthalassa. Scientific Reports 3, 1889, 1-6.

Nozaki, T., Kato, Y., Suzuki, K., 2014. Re-Os geochronology of the Hitachi volcanogenic massive sulfide deposit: The oldest ore deposit in Japan. Economic Geology 109, 2023-2034.

Okay, A.I., 2000. Was the Late Triassic orogeny in Turkey caused by the collision of an ocean plateau?, in: Bozkurt, E., Winchester, J.A., Piper, J.D.A. (Eds.), Tectonics and Magmatism in Turkey and the Surrounding Area. Geological Society, London, Special Publication 173, pp. 25-41.

Okay, A.I., Göncüoğlu, M.C., 2004. The Karakaya Complex: A review of data and concepts. Turkish Journal of Earth Sciences 13, 77-95.

Okay, A.I., Mostler, H., 1994. Carboniferous and Permian radiolarite blocks from the Karakaya Complex in northwest Turkey. Turkish Journal of Earth Sciences 3, 23-28.

Okay, A.I., Satır, M., Maluski, H., Siyako, M., Monie, P., Metzger, R., Akyüz, S., 1996. Palaeo- and Neo-Tethyan events in northwestern Turkey: geology and geochronologic constraints, in: Yin, A., Harrison, T.M. (Eds.), The tectonic evolution of Asia. Cambridge University Press, Cambridge-New York-Melbourne, pp. 420-441.

Okay, A.I., Tüysüz, O., 1999. Tethyan sutures of northern Turkey, in: Durand, B., Jolivet, L., Horváth, F., Séranne, M. (Eds.), The Mediterranean Basins: Tertiary Extension with the Alpine Orogen. Geological Society, London, Special Publication 156, pp. 475-515.

Önder, F., Boztuğ, D., Yılmaz, O., 1987. New paleontological (Conodont) from the Lower Mesozoic rocks of the Göynükdağı-Kastamonu region at the Western Pontides, Turkey. Melih Tokay Geology Symposium, Ankara, Abstracts, 127-128 (in Turkish).

Pehlivanoğlu, H., 1985. Kastamonu-Küre Piritli Bakır Yatakları ve Çevresi Hakkında Jeoloji Raporu. Mineral Research and Exploration Institute of Turkey (MTA) Report 1744 (unpublished).

Peucker-Ehrenbrink, B., Jahn,B.-m, 2001. Rhenium-osmium isotope systematic and platinum group element concentrations: Loess and the upper continental crust, Geochemistry Geophysics Geosystems 2 (10), doi:10.1029/2001GC000172.

Pickett, E.A., Robertson, A.H.F., 1996. Formation of the Late Palaeozoic-Early Mesozoic Karakaya Complex in NW Turkey by Palaeotethyan subduction-accreation. Journal of Geological Society, London 153, 995-1009.

Pickett, E.A., Robertson, A.H.F., Dixon, J.E., 1995. The Karakaya Complex, NW Turkey: a Palaeotethyan accreationary complex, in: Erler, A., Ercan, T., Bingöl, E. Örçen, S. (Eds.), Geology of the Black Sea region. General Directorate of Mineral Research and Exploration & Chamber of Geological Engineers, 11-18, Ankara.

Piercey, S.J., 2010. An overview of petrochemistry in the regional exploration for volcanogenic massive sulphide (VMS) deposits. Geochemisty: Exploration, Environment, Analysis 10,119–136.

Piercey, S.J., 2011. The setting, style, and role of magmatism in the formation of volcanogenic massive sulfide deposits. Mineralium Deposita 46, 449-471.

Pirajno, F., 2009. Hydrothermal Processes and Mineral Systems. Springer, Berlin, 1250p.

Ravizza G., Turekian, K.K., 1989. Application of the ^{187}Re-^{187}Os system to black shale geochronometry. Geochimica et Cosmochimica Acta 53 (12), 3257-3262.

Ravizza G., Turekian, K.K., Hay, B.J., 1991. The geochemistry of rhenium and osmium in recent sediments from the Black Sea. Geochimica et Cosmochimica Acta 55 (12), 3741-3752.

Robertson, A.H.F., Ustaömer, T., 2009. Tectonic development of the Black Sea in the Eastern and Central Pontides, Turkey: framework for opening of the Eastern Black Sea Basin. Abstracts of the 2nd International Symposium on the Geology of the Black Sea Region. 5-9 October 2009, Ankara.http://eski.jmo.org.tr/resimler/ekler/99430bd25e315dd_ek.pdf, last accessed November 25th, 2015, 10:48 AM.

Sarıcan, K., 1968. Bakibaba cevher yatağı arama ve değerlendirme çalışmaları raporu, Küre: Etibank KBİ Rep. (unpublished).

Sarıfakıoğlu, E., Sevin, M., Dilek, Y., 2013. Remnant of a Jurassic backarc ocean basin (Küre Ophiolite) in the Central Pontide Belt, Turkey. Geological Society of America Cordilleran Section Meeting, Fresno, California, 20-22 May 2013, Abstracts v.45, No. 6, p.72.

Sawkins, F.J., 1976. Massive sulphide deposits in relation to geotectonics. Geol. Assoc. Can. Spec. Pap. 14, 221-240.

Schwartz, M.O., 2000. Cadmium in zinc deposits: Economic geology of a polluting element. International Geology Review 42, 445-469.

Selby, D., Creaser, R.A., 2003. Re–Os geochronology of organic rich sediments: an evaluation of organic matter analysis methods. Chemical Geology 200 (3-4), 225-240.

Selby D., Kelley K. D., Hitzman M. W., Zieg J., 2009. Re–Os sulfide (bornite, chalcopyrite, and pyrite) systematics of the carbonate-hosted copper deposits at Ruby Creek, southern Brooks Range, Alaska. Economic Geology 104, 437–444.

Shepherd, T.J., Rankin, A.H., Alderton, D.H.M., 1985. A Practical Guide to Fluid Inclusion Studies. Blackie & Son Ltd., Glasgow & London, 240 pp.

Singh, S.K., Trivedi, J.R., Krishnaswami, S., 1999. Re-Os isotope systematics in black shales from the Lesser Himalaya: Their chronology and role in the $^{187}Os/^{188}Os$ evolution of sea-water. Geochimica et Cosmochimica Acta 63, 2381-2392.

Suzuki K., Shimizu H., Masuda A., 1996. Re–Os dating of molybdenites from ore deposits in Japan: implication for the closure temperature of the Re–Os system for molybdenite and the cooling history of molybdenum ore deposits. Geochimica et Cosmochimica Acta 60, 3151–3159.

Stampfli, G.M., Borel, G.D., Marchant, R., Mosar, J., 2002. Western Alps geological constraints on western Tethyan reconstructions. In: Rosenbaum, G. and Lister, G.S. (eds.), Reconstruction of the evolution of the Alpine-Himalayan Orogen, Journal of the Virtual Explorer 8, 77-106.

Steele-MacInnis, M., Han., L., Lowell, R.P., Rimstidt, J.D., Bodnar, R.J., 2012. Quartz previpitation and fluid inclusion characterstics in sub-seafloor hydrothermal systems associated with volcanogenic massive sulfide deposits. Central European Journal of Geosciences 4(2), 275-286. DOI: 10.2478/s13533-011-0053-z.

Stein H.J., Morgan, J.W., Scherstén A., 2000. Re–Os dating of low-level highly radiogenic (LLHR) sulfides: the Harnäs gold deposit, southwest Sweden, records continental-scale tectonic events. Economic Geology 95, 1657–1671.

Şengör, A.M.C., 1979. The North Anatolian Trasnform Fault: Its age, offset and tectonic significance. Journal of the Geological Society, London 136, 269-282.

Şengör, A.M.C., 1984. The Cimmeride orogenic system and the tectonics of Eurasia. Geological Society of America Special Paper 195, 82p.

Şengör, A.M.C., 1985. Die Alpinden und die Kimmeriden: Die verdoppelte Geschichte der Tethys. Geologische Rundschau 74, 181-213.

Şengör, A.M.C., Yılmaz, Y., 1981. Tethyan evolution of Turkey: a plate tectonic approach. Tectonophysics 75, 181-213.

Şengör, A.M.C., Yılmaz, Y., Ketin, İ., 1980a. Remnants of a pre-Late Jurassic ocean in northern Turkey, Fragments of Permo-Triassic Paleo-Tethys?. Geological Society of America Bulletin 91, 599-609.

Şengör, A.M.C., Yılmaz, Y., Ketin, İ., 1980b. Remnants of a pre-Late Jurassic ocean in northern Turkey, Fragments of Permo-Triassic Paleo-Tethys?: Discussion and Reply, Geological Society of America Bulletin 93, 929-936.

Şengör, A.M.C., Yılmaz, Y., Sungurlu, O., 1984. Tectonics of the Mediterranean Cimmerides: nature and evolution of the western termination of Palaeo-Tethys, in: Dixon, J.E., Robertson, A.H.F. (Eds.), The Geological Evolution of the Eastern Mediterranean. Geological Society, London, Special Publication 17, 77-112.

Tejada, M.L.G., Suzuki, K., Kuroda, J., Coccioni, R., Mahoney, J.J., Ohkouchi, N., Sakamoto, T., Tatsumi, Y., 2009. Ontong Java Plateau eruption as a trigger for the early Aptian oceanic anoxic event. Geology 37, 855-858.

Terakado, Y., 2001a. Re-Os dating of the Kuroko ores from the Wanibuchi Mine, Shimane Prefecture, southwestern Japan. Geochemical Journal 35, 169-174.

Terakado, Y., 2001b. Re-Os dating of the Kuroko ore deposits from the Hokuroku district, Akita Prefecture, Northeast Japan. Jour. Geol. Soc. Japan 107, 354–357.

Terzioğlu, N.M., Satır, M., Saka, K., 2000. Geochemistry and geochronology of basaltic rocks of the Küre Basin, Central Pontides (N-Turkey). International Earth Sciences Colloquium on the Aegean Region IESCA-2000, 25-29 September 2000, Izmir, Turkey, Abstracts, p. 219.

Turekian, I.K., Wedepohl, K.H., 1961. Distribution of the elements in some major units of the earth’s crust. The Geological Society of America Bulletin 72, 175–192.

Tüysüz, O., 1986. Kuzey Anadolu'da iki farklı ofiyolit topluluğu: Eski ve Yeni Tetisin artıkları: Tübitak Doğa Mühendislik and Çevre Bilimleri Dergisi 10 (2), 172-179.

Ustaömer, T., Robertson, A.H.F., 1993. Late Palaeozoic–Early Mesozoic marginal basins along the active southern continental margin of Eurasia: evidence from the Central Pontides (Turkey) and adjacent regions. Geological Journal 28, 219–238.

Ustaömer, T., Robertson, A.H.F., 1994. Late Palaeozoic marginal basin and subduction-accreation: the Palaeotethyan Küre Complex, Central Pontides, northern Turkey. Journal of the Geological Society, London 151, 291-305.

Ustaömer, T., Robertson, A.H.F., 1995. Palaeotethyan tectonic evolution of the North Tethyan Margin in the Central Pontides, N. Turkey, in: Erler, A., Ercan, T., Bingöl, E., Örçen, S. (Eds)., Proceedings of the International Symposium on the Geology of the Black Sea Region. Mineral Research and Exploration Institute of Turkey (MTA): Ankara; pp. 24–32.

Ustaömer, T., Robertson, A.H.F., 1999. Geochemical evidence used to test alternative plate tectonic models for pre-Upper Jurassic (Palaeotethyan) units in the Central Pontides, N Turkey, Geological Journal 34, 25-23.

Ustaömer, T., Robertson, A.H.F., 1997. Tectonic-sedimentary evolution of the north Tethyan margin in the central Pontides of northern Turkey, in: Robinson AG (Ed.), Regional and Petroleum Geology of the Black Sea and Surrounding Region. American Association of Petroleum Geologists Memoir 68, pp. 255–290.

Vinogradov, A.P., 1962. Die Durchschnittsgehalte der chemischen Elemente in den Hauptarten der Eruptivgesteine. Geochimija 7 (in Russian).

Walker R. J., Morgan J. W., Horan M. F., Czamanske G. K., Krogstad E. J., Fedorenko V. A., Kunilov V. E., 1994. Re–Os isotopic evidence for an enriched-mantle source for the Noril´sk-type, ore-bearing intrusions, Siberia. Geochimica et Cosmochimica Acta 58, 4179–4197.

Xu, G., 1998. Geochemistry of sulphide minerals at Dugald River, NW Queensland, with reference to ore genesis. Mineralogy and Petrology 63, 119-139.

Xuexin, S., 1984. Minor elements and ore genesis of the Fankou lead-zinc deposit, China, Mineralium Deposita 19, 95-104.

Yiğit, Ö., 2011. Mineral exploration: What, where and why in Turkey. Mining Turkey 1, 12-19.

Yiğit, Ö., 2009. Mineral deposits of Turkye in relation to Tethyan Metallogeny: Implications for future mineral exploration. Economic Geology 104, 19-51.

Yiğit, Ö., 2006. Gold in Turkey – a missing link in Tethyan metallogeny. Ore Geology Reviews 28, 147-179.

Yiğitbaş, E., Elmas, A., Yılmaz, Y., 1999. Pre-Cenozoic tectono-stratigraphic components of the Western Pontides and their geological evolution. Geological Journal 34, 55-74.

Yiğitbaş, E., Kerrich, R., Yılmaz, Y., Elmas, A., Xie, Q.L., 2004. Characteristics and geochemistry of Precambrian ophiolites and related volcanics from the Istanbul–Zonguldak Unit, Northwestern Anatolia, Turkey: following the missing chain of the Precambrian South European suture zone to the east. Precambrian Research 132, 179–206.

Yılmaz, O., 1979. Daday-Devrekani Masifi Kuzeydoğu Kesimi Metamorfik Petrolojisi. Doçentlik Tezi, Hacettepe Üniversitesi, Jeoloji Mühendisliği Bölümü, Ankara, 176p (in Turkish).

Yılmaz, O., 1980. Lithostratigraphic units and tectonics of Northeastern part of the Daday Devrekani Massif (Western Pontides, Turkey). Publication of Institute of Earth Sciences of Hacettepe University 5–6, 101–135 (in Turkish with English abstract).

Yılmaz, Y., Şengör, A.M.C., 1985. Palaeo-Tethyan ophiolites in northern Turkey: petrology and tectonic setting. Ofioliti 10, 485–504.

Yılmaz, Y., Genç, S.C., Yigitbaş, E., Bozcu, M.,Yılmaz, K., 1994a. Kuzeybatı Anadoluda Geç Kretase yaşlı kıta kenarının jeolojik evrimi. Proceedings of the 10th Petroleum Congress of Turkey, p. 37-55.

Yılmaz, Y., Genç, S.C., Yigitbaş, E., Bozcu, M., Yılmaz, K., 1994b. Geological evolution of the late Mesozoic continental margin of northwestern Anatolia. Tectonophysics 243, 155-171.

Yılmaz, Y., Tüysüz, O., Yiğitbaş, E., Genç, Ş.C., Şengör, A.M.C., 1997. Geology and tectonic evolution of the Pontides, in: Robinson, A.G. (Ed.), Regional and Petroleum Geology of the Black Sea and Surrounding Regions. American Association of Petroleum Geologists Memoir 68, 183–226.

Yu, G., Yang, G., Chen, J.F., Qu W.J., Du., A.D., He, W., 2005. Re-Os dating of gold-bearing arsenopyrite of the Maoling gold deposit, Liaoning Province, Northeast China and its geological significance. Chinese Science Bulletin 50, 1509–1514.

Zaw, K., Large, R.R., 1996. Petrology and geochemistry of sphalerite from the Cambrian VHNS deposits in the Rosebery-Hercules district, western Tasmania: implications for gold mineralisation and Devonian metamorphism-metasomatic processes. Mineralogy and Petrology 57, 97-118.

Zhu, B., Becker, H., Jiang, S.-Y., Pi, D.-H., Fischer-Gödde, M., Yang, J.-H., 2013. Re-Os geochronology of black shales from the Neoproterozoic Doushantuo Formation, Yangtze platform, South China. Precambrian Research 225, 67-76.

Figure Captions

Figure 1. (a) Distribution of submarine volcanic, ophiolitic and acidic to intermediate intrusive host rock assemblages and related VMS and Porphyry Deposits of Turkey, with respect to the Paleo-tectonic units (after Yigit, 2009). STZ: Strandja Zone, WP: Western Pontides, CP: Central Pontides, EP: Eastern Pontides, BFZ: Bornova Flysch Zone, TZ Tavşanlı Zone, MM: Menderes Massif, MTP: Menderes-Taurus Platform, AZ: Afyon Zone; CACC: Central Anatolian Crystalline Complex, EAAC: Eastern Anatolian Accretionary Complex, IAES: İzmir-Ankara-Erzincan Suture, BS: Bitlis Suture, IPS: Intra-Pontide Suture. (b) Regional Geological Map of the Küre and surroundings (modified after Aydın et al., 1995; Kozur et al., 2000). Fm: formation, M: member, Gr: Group.

Figure 2. (a) Geological map of the Küre VMS deposit and its surroundings (after Güner, 1980; Pehlivanoğlu, 1985; JICA and MMAJ, 1992; Çakır, 1995 and Çakır et al., 2006). (b) Generalized columnar section of the Küre ophiolite (modified after Ustaömer and Robertson, 1994).

Figure 3. (a) and (b) shows a general view of the Bakibaba Open-pit during the field studies in 2012, (b) and (c) steeply inclined contact of the Black shale-subgraywacke unit (Bs-Sg) and the pillow lavas (Pl). (d) Pillow lava outcrop from the Bakibaba Open-pit. (e) Black shale-subgraywacke on bench face from the Bakibaba Open-pit. (f) Close-up view of the vertical segment of the black shale-subgraywacke - pillow lava contact.

Figure 4. Photomicrographs of the (a and b) fresh (unaltered) and (c, d, e, f) altered (heavily chloritized) basaltic pillow lavas. Note the overprinting quartz and calcite stockwork veinlets in (c, d, e and f). Cpx: clinopyroxene, Plg: plagioclase, Chl: chlorite, Qz: quartz, Ca:calcite. Op: opaque phases. Photomicrographs (a, b, e and f) are in (+), (c, d) are in (//) nicols.

Figure 5. A schematic summary of the sample depths, types, and lithologies. N-S oriented cross-section of the Mağaradoruk mineralization is from Altun et al. (2015).

Figure 6. Reflected-light images of the ore minerals from massive and stockwork ores of sulfide mineralization. (a) Magnetite (Mgt) replaced by hematite (Hm). (b) Flaky and needle-like and/or acicular hematite (Hm) in euhedral pyrite and the quartz veinlet in the stockwork ore. (c) Subhedral/anhedral pyrite (Py) accumulations embedded in chalcopyrite-I (CcpI). (d) Subhedral/anhedral pyrite (Py) accumulations embedded in manly sphalerite-I (SphI) that include exsolutions/inclusions and/or rhythmic bandings of chalcopyrite-II(CcpII) and chalcopyrite-I (CcpI). (e) Subhedral pyrite (Py) replaced by chalcopyrite-I (CcpI), that is further replaced by sphalerite-I (SphI) and chalcopyrite-II (CcpII). (f) Chalcopyrite-I (CcpI) and bornite (Bo) inter-growths replacing pyrite (Py) and being replaced by sphalerite-II (SphII). (g) Chalcopyrite exsolution lamellae (CcpII) in bornite (Bo). (h) Euhedral/subhedral cobaltite (Co)-pyrite (Py) intergrowths, being replaced by chalcopyrite-I (CcpI). Note the bravoite (Brv) zoning in pyrite (Py). All photomicrographs are in (//) nicols. Images (a), (g) and (h) are in oil immersion.

Figure 7. Reflected-light images of the ore minerals from massivesulfide mineralization. (a) Cobaltite (Co)-pyrite (Py) intergrowths is being replaced by chalcopyrite-I (CcpI) that is further replaced by melnicovite pyrite (Mel-Py). (b) Pyrite (Py) being replaced by chalcopyrite-I (CcpI) and sphalerite-I (SphI). Chalcopyrite is further replaced by melnicovite pyrite (Mel-Py) and marcasite (Mrc). (c) Replacement of melnicovite pyrite (Mel-Py) by marcasite (Mrc). Marcasite is followed by sphalerite-I (SphI) that include chalcopyrite-II (CcpII) exsolution lamella. (d) Native gold (Au) at the boundary of pyrite (Py) and chalcopyrite-I (CcpI). (e) and (f) Native gold (Au) as minute inclusions in pyrite. All images are in (//) nicols. Images (c) and (d) are in oil immersion.

Figure 8. Zn/Cd distributions of sphalerites from Küre VMS Deposit (*) with the data from different ore-forming systems and source rocks. Reference data are: (1) Xu, 1998; (2) Jonasson and Sangster, 1978; (3) Xuexin, 1984;(4) Brill, 1989; (5) Zaw and Large, 1996; (6)

Gottesman and Kampe, 2007; (7) Goodfellow and Blaise, 1988;(8) Goodfellow and Franklin, 1993; (9) Hannington and Scott, 1988; (10) Bischoff et al., 1983; (11) Fouquet et al., 1993;(12) Turekian and Wedepohl, 1961; (13) Vinogradov, 1962; (14) Kay and Hubbard, 1978, (15) Herzig, 1988. Filled squares represent sphalerite data from massive ore of Küre deposit. Zn/Cd interval scheme adapted and modified from Gottesman and Kampe (2007).

Figure 9. Photomicrographs of the veinlets and the hosted fluid inclusions in the stockwork zone of the Küre massive sulfide mineralization. (a) to (d) show early and late stage quartz veinlets (Qz1 and Qz2, respectively) and , (1a) and (1b) represents early and late stage in the (Qz1). (e), (f) and (g) show samples of two phase fluid inclusions from the quartz veinlets of the stockwork ore, (L and V denotes liquid and vapor phases respectively).

Figure 10. A diagram-histogram composite of homogenization temperatures (T_h) and the fluid salinities obtained by the microthermometric measurements from the quartz of the stockwork ore of the Küre VMS deposit.

Figure 11. (a) ^{187}Re-^{188}Os vs. ^{187}Os-^{188}Os plot for all of the six Küre VMS pyrite concentrates. (b) ^{187}Re-^{188}Os vs. ^{187}Os-^{188}Os iscochron for four of the pyrite concentrates. (c) ^{187}Re-^{187}Os^{r} isochron for the same set of pyrite concentrates. (d) Weighted average of the model ages plotted for the Küre VMS deposit samples. The data-point error ellipses in (a), (b) and (c), and the box heights in (d) donate 2SE.

Figure12. (a) Tectonic map of northern Anatolia showing the distribution of the Late Triassic-Early Jurassic Paleo-Tethyan accretionary complex and ophiolite (Karakaya-Küre) (from Okay and Göncüoğlu, 2004). Light grey shaded region shows the Pontides. CP: Central Pontides, EP: Eastern Pontides, IAES: İzmir-Ankara-Erzincan Suture, IPS: Intra-Pontide Suture. (b) Schematic cartoon depicting the western Tethyan realm during Early Norian (from Stampfli et al., 2002). (Bd) Beydağları; (Is) Istanbul; (Kk) Karakaya forearc; (KS) Kotel-Stranja rift; (Mn) Menderes; (Pl) Pelagonian; (Rh) Rhodope; (Sc) Scythian platform; (Sk)

Sakarya; (TD) Trans-Danubian. (c) Summary of the Geological history of the volcano-sedimentary associations of Küre Complex and the Küre VMS Deposit. Reference data are from: (1) Kozur et al. (2000); (2) Aydın et al. (1995); (3) Terzioğlu et al. (2000); (4) Ustaömer and Robertson (1995); (5) Alişan et al. (1992); (6) Çakır (1995); (*)This study.

Table Captions

Table 1. Selected compositional (EPMA) data from some of the main ore phases (pyrite, chalcopyrite, sphalerite) in the Küre VMS deposit.

Table 2. Microthermometric measurements from the quartz of the stockwork ore of the Küre VMS deposit.

Table 3. The Re and Os concentrations and isotope compositions of the six separated pyrite-rich concentrates and two black shale samples.

Figure 1

Click here to download Figure: Figure 1.pdf

Figure 1

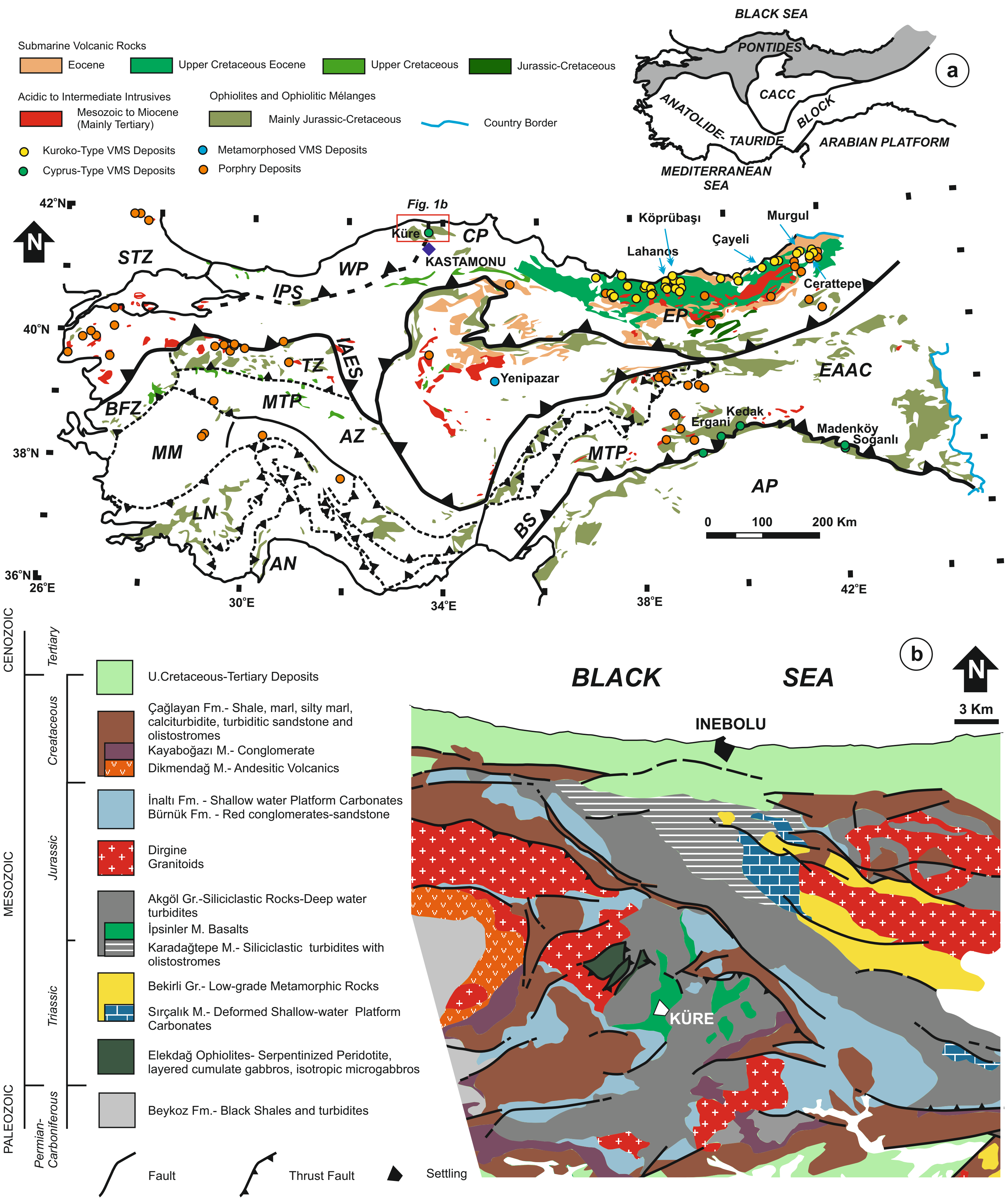

Figure 2
Click here to download Figure: Figure 2.pdf

Figure 2

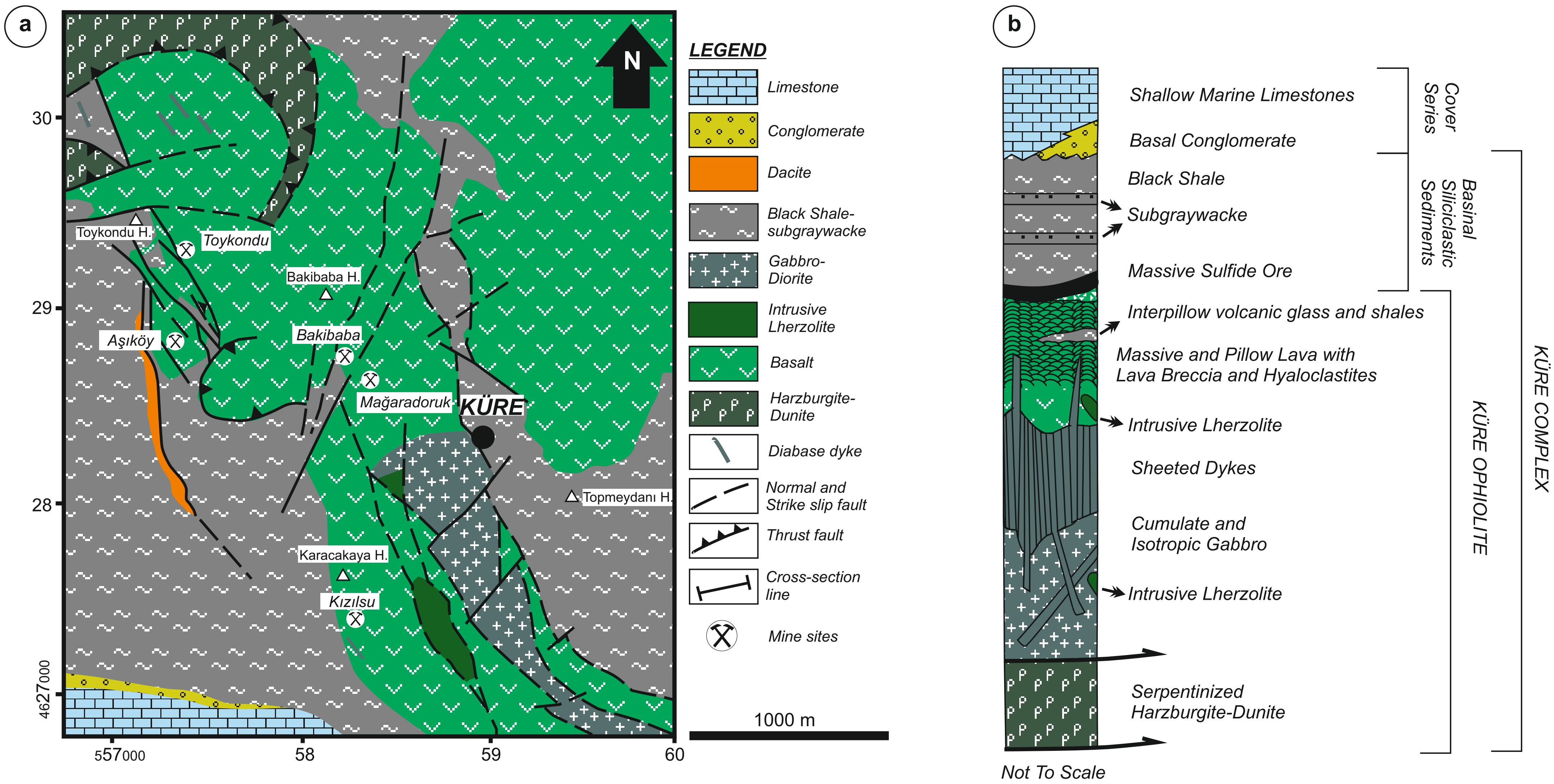

Figure 3
Click here to download high resolution image

Figure 3

Figure 4
Click here to download high resolution image

Figure 4

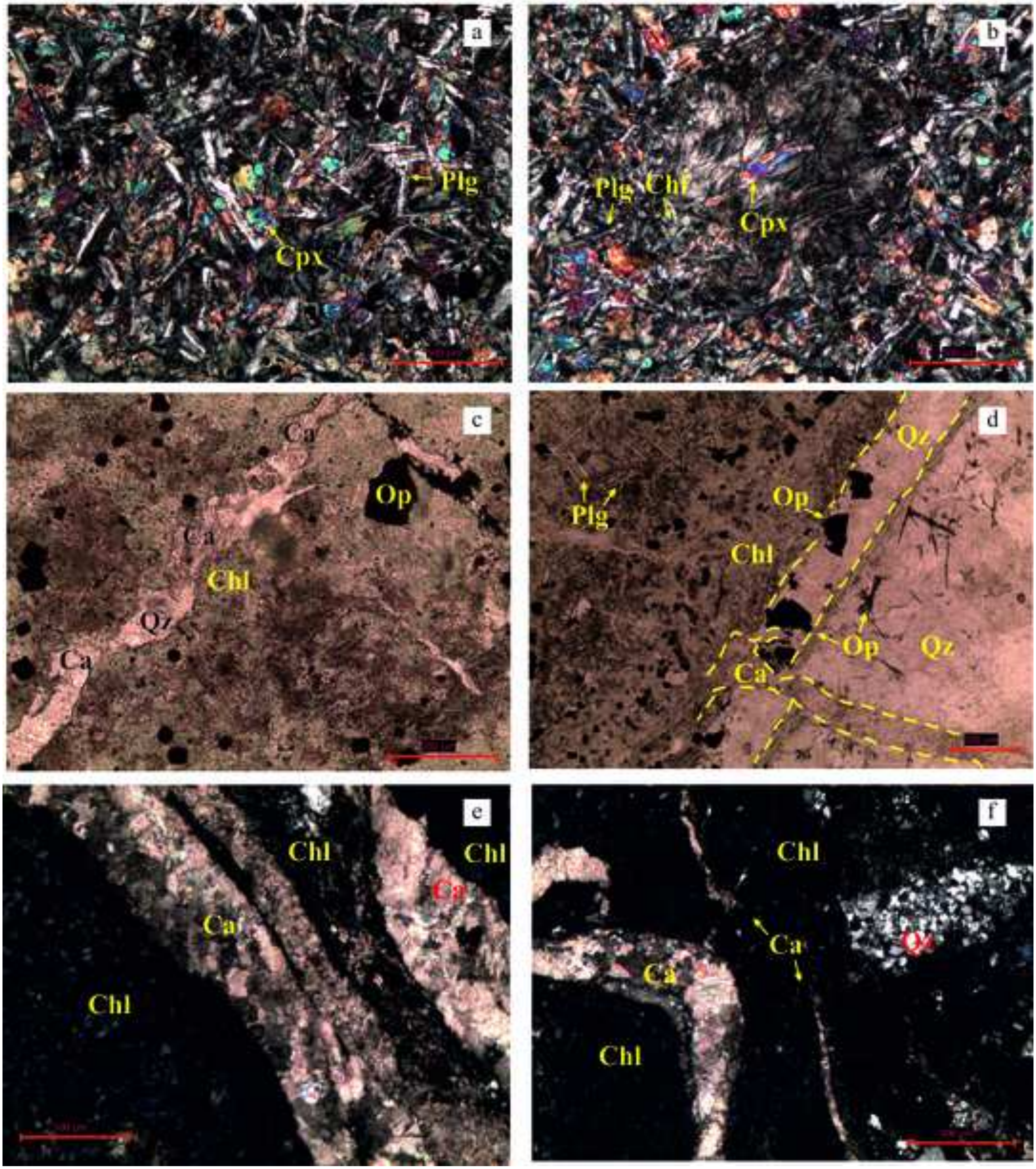

Figure 5
Click here to download high resolution image

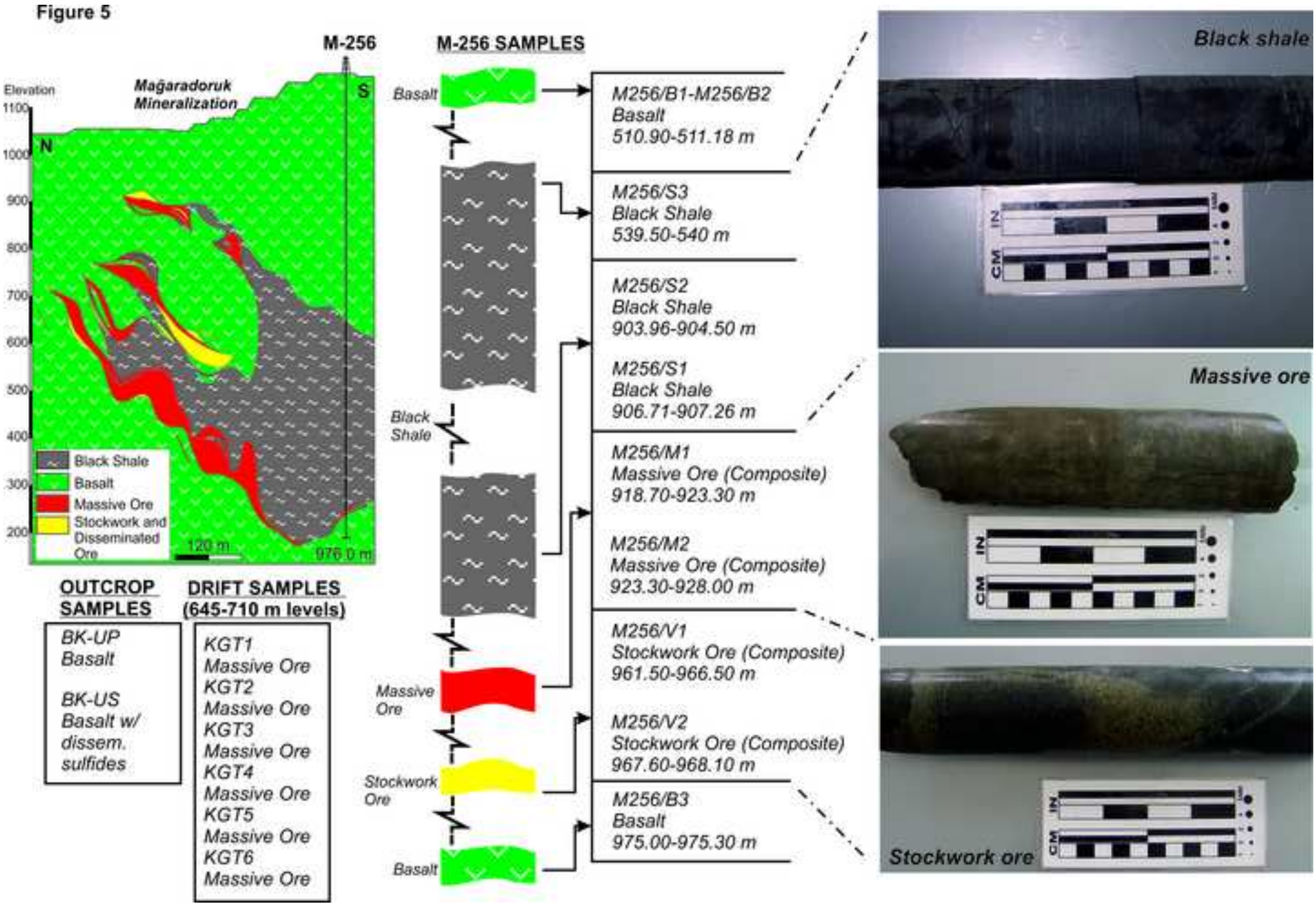

Figure 6
Click here to download high resolution image

Figure 6

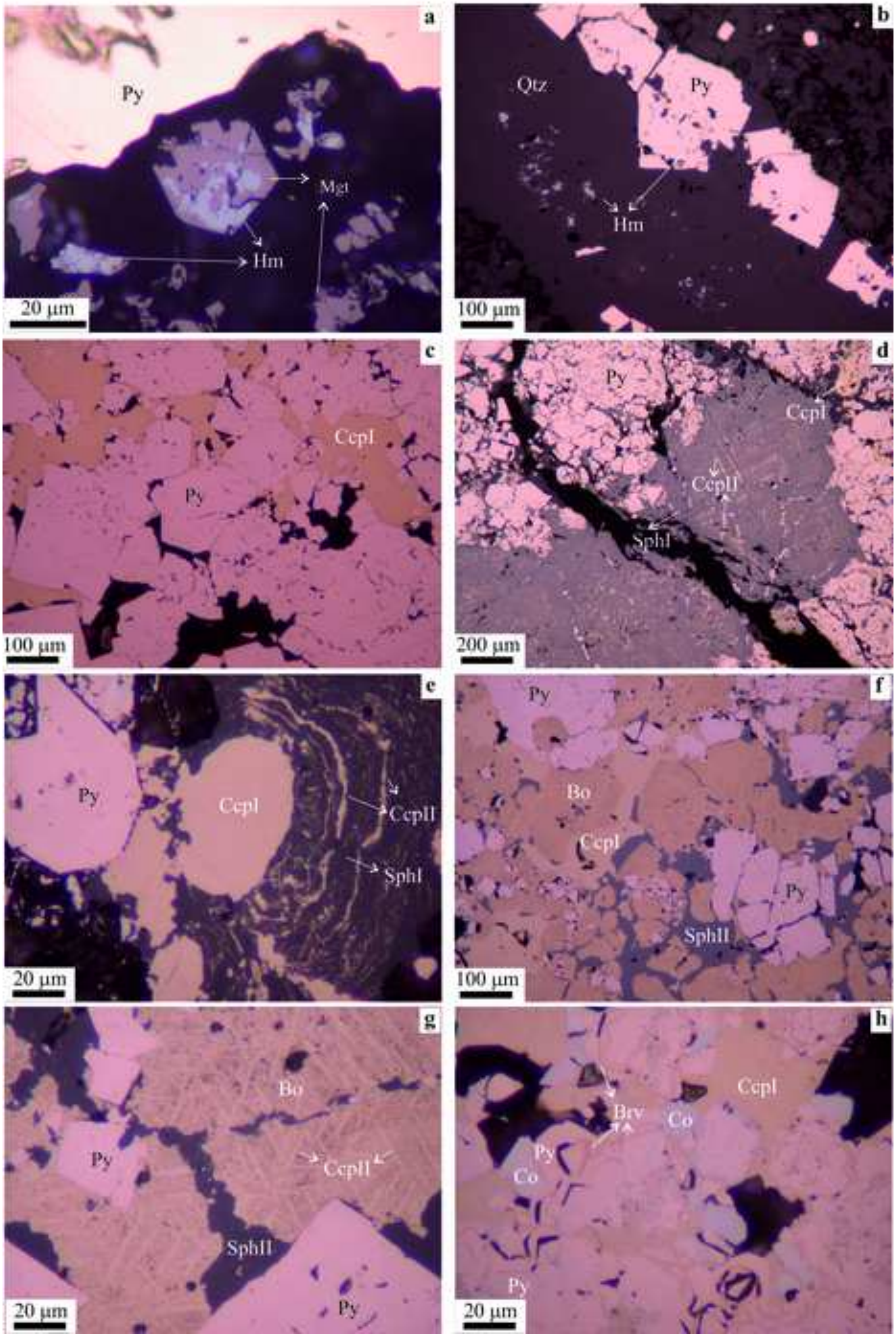

Figure 7
Click here to download high resolution image

Figure 7

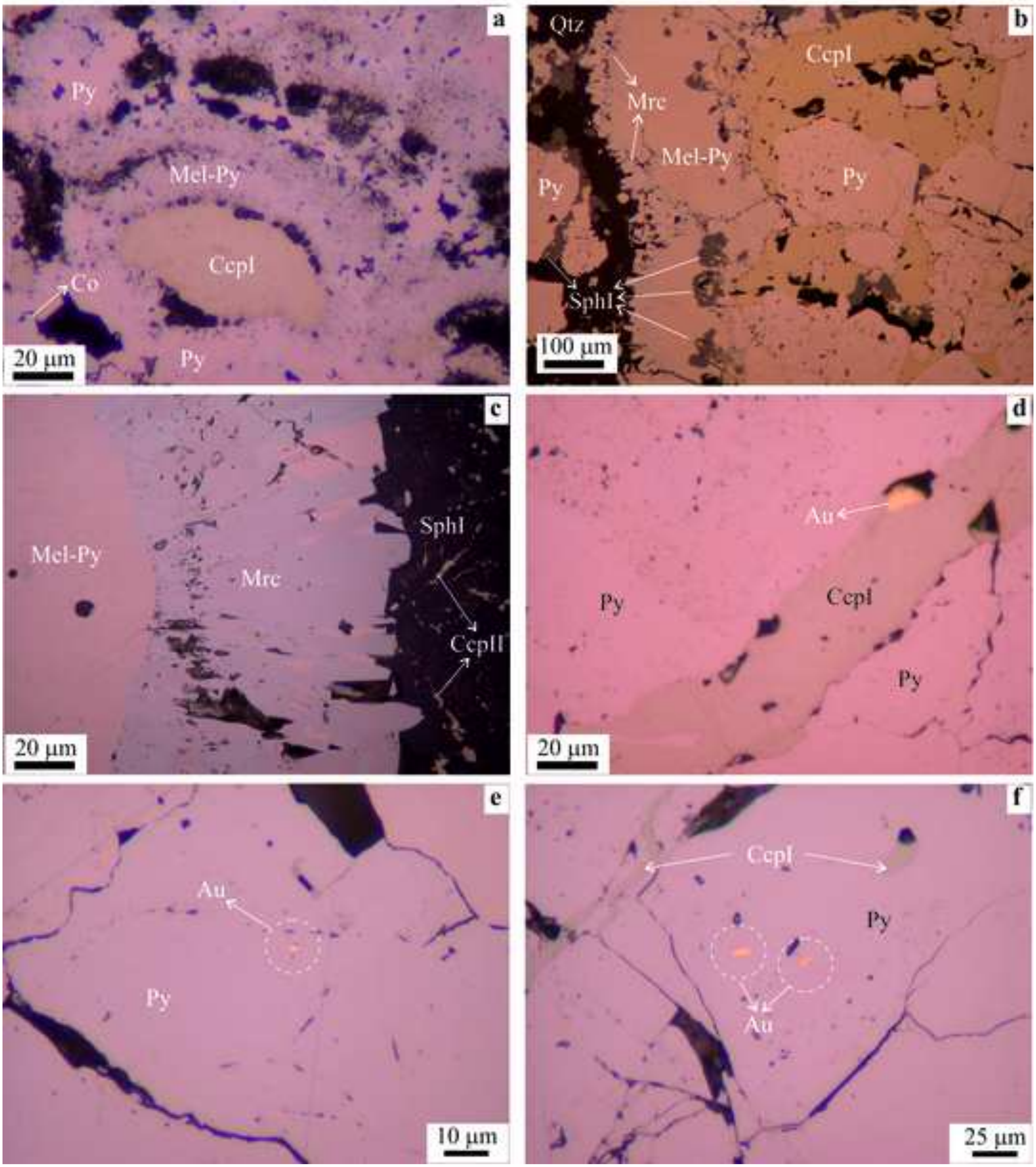

Figure 8
Click here to download Figure: Figure 8.pdf

Figure 8

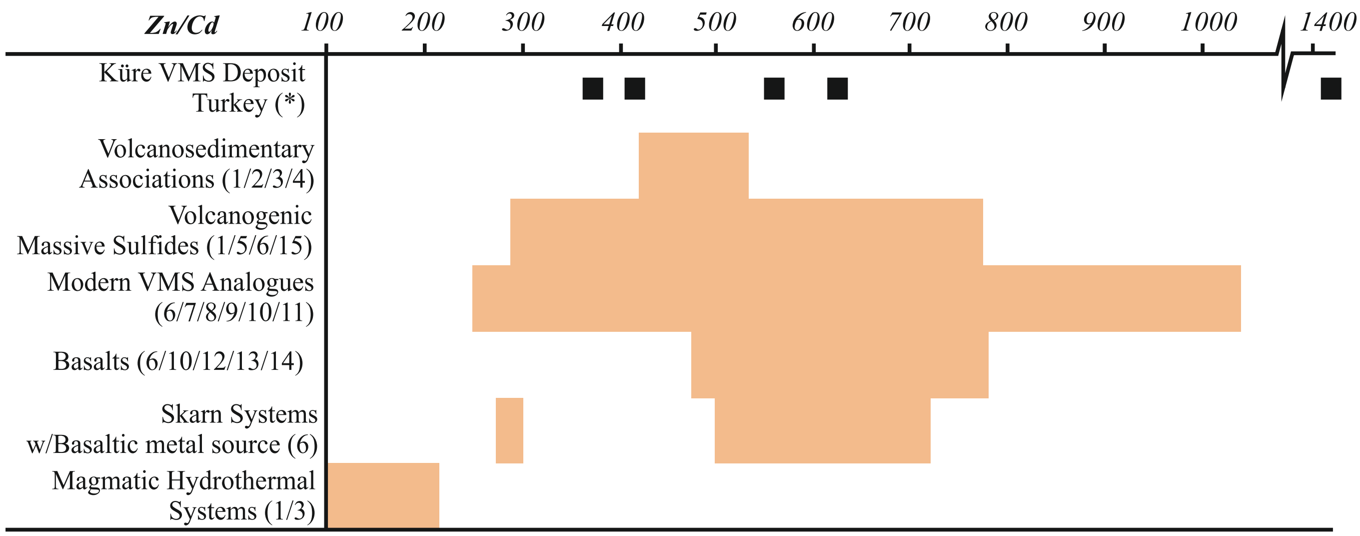

Figure 9
Click here to download high resolution image

Figure 9

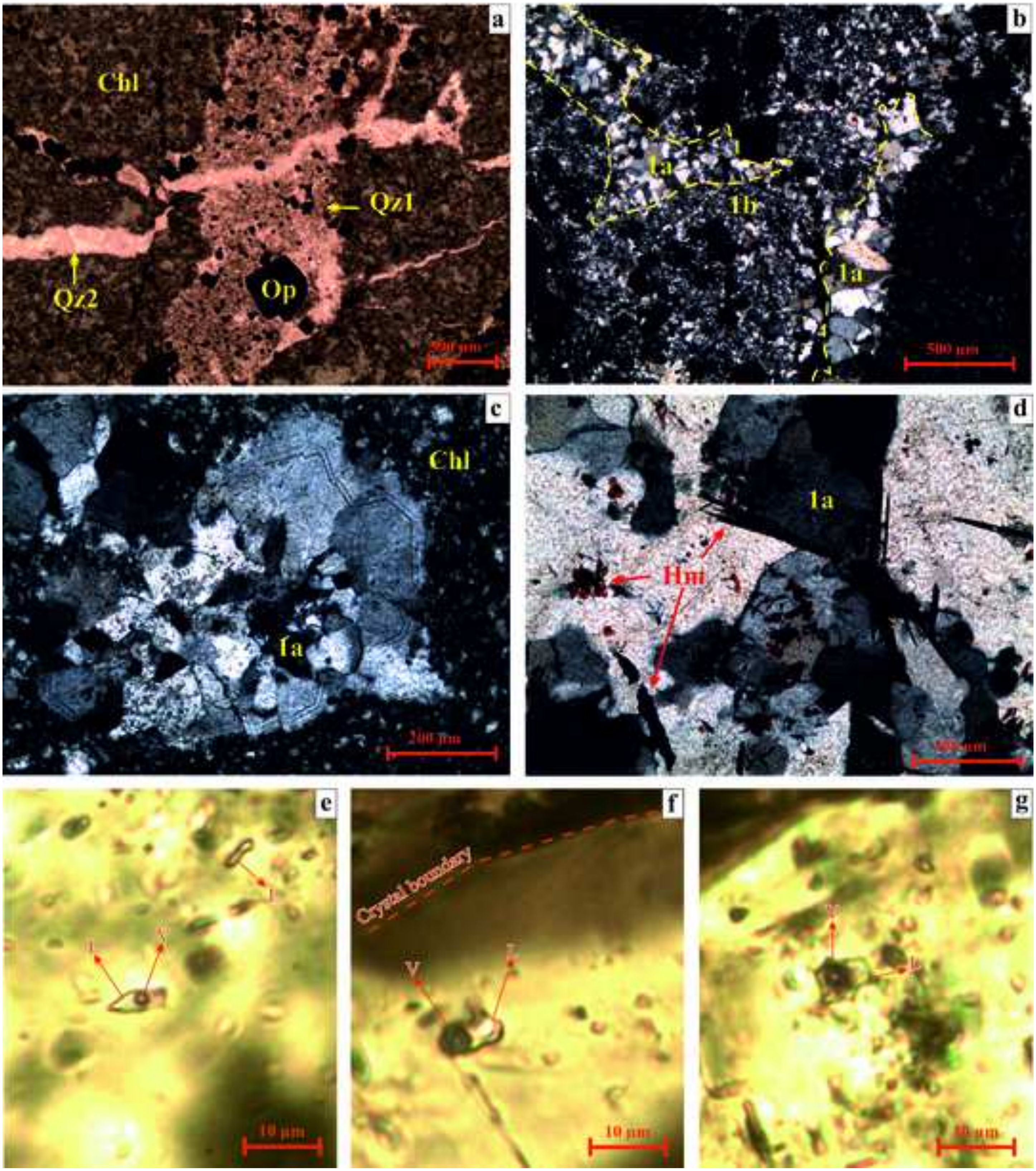

Figure 10
Click here to download Figure: Figure 10.pdf

Figure 10

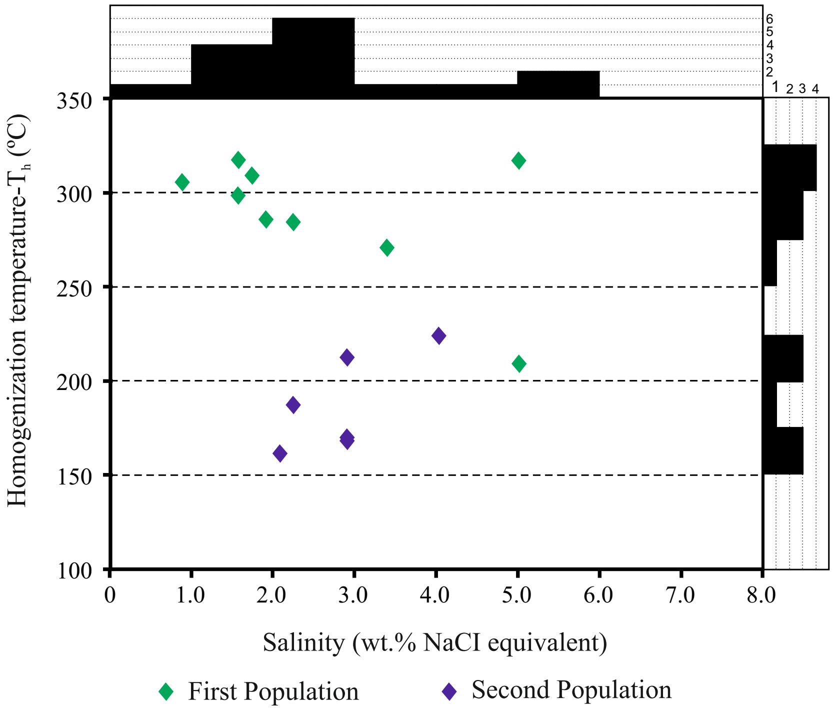

Figure 11
Click here to download Figure: Figure 11.pdf

Figure 11

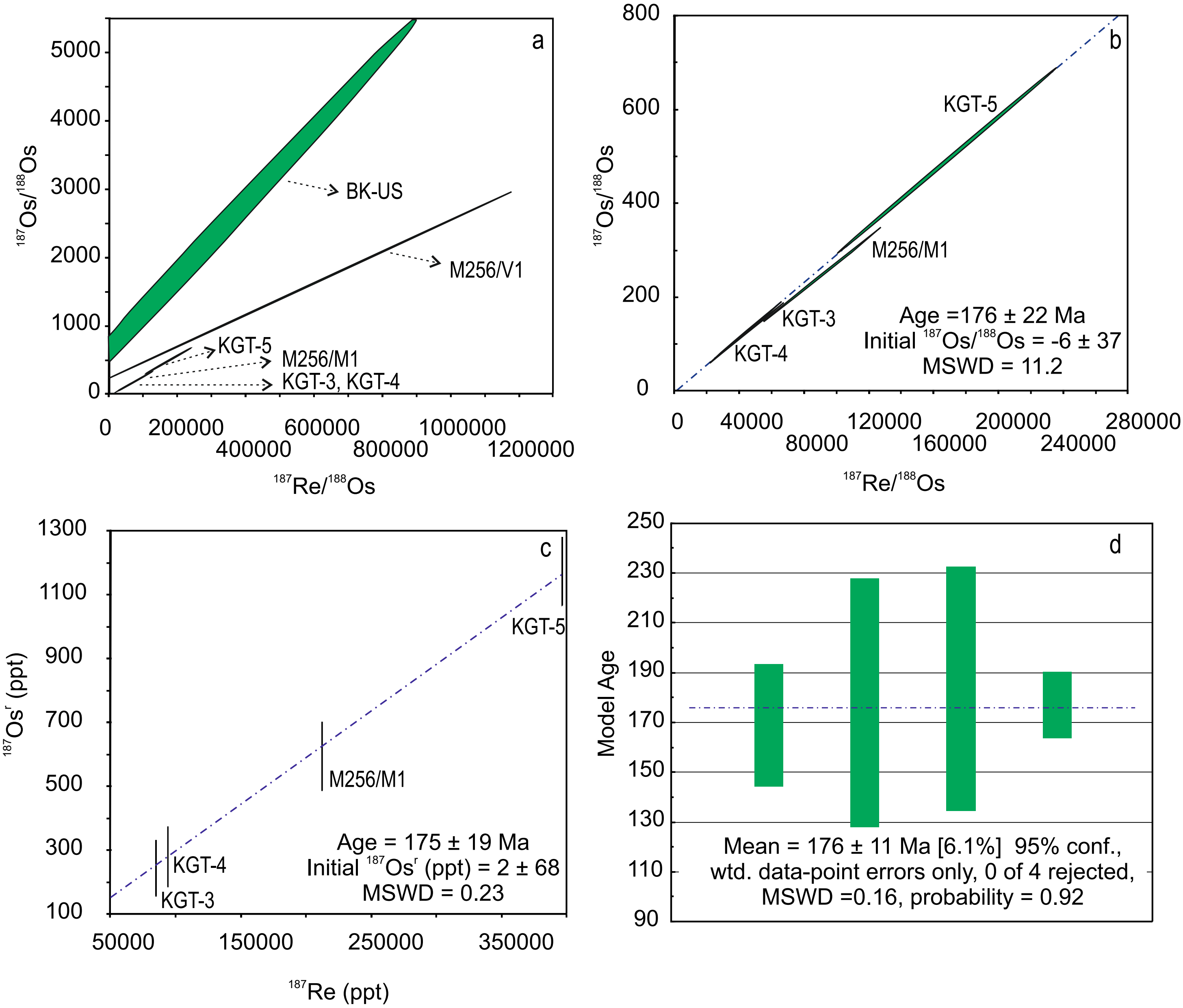

Figure 12
Figure 12
Click here to download Figure: Figure 12.pdf

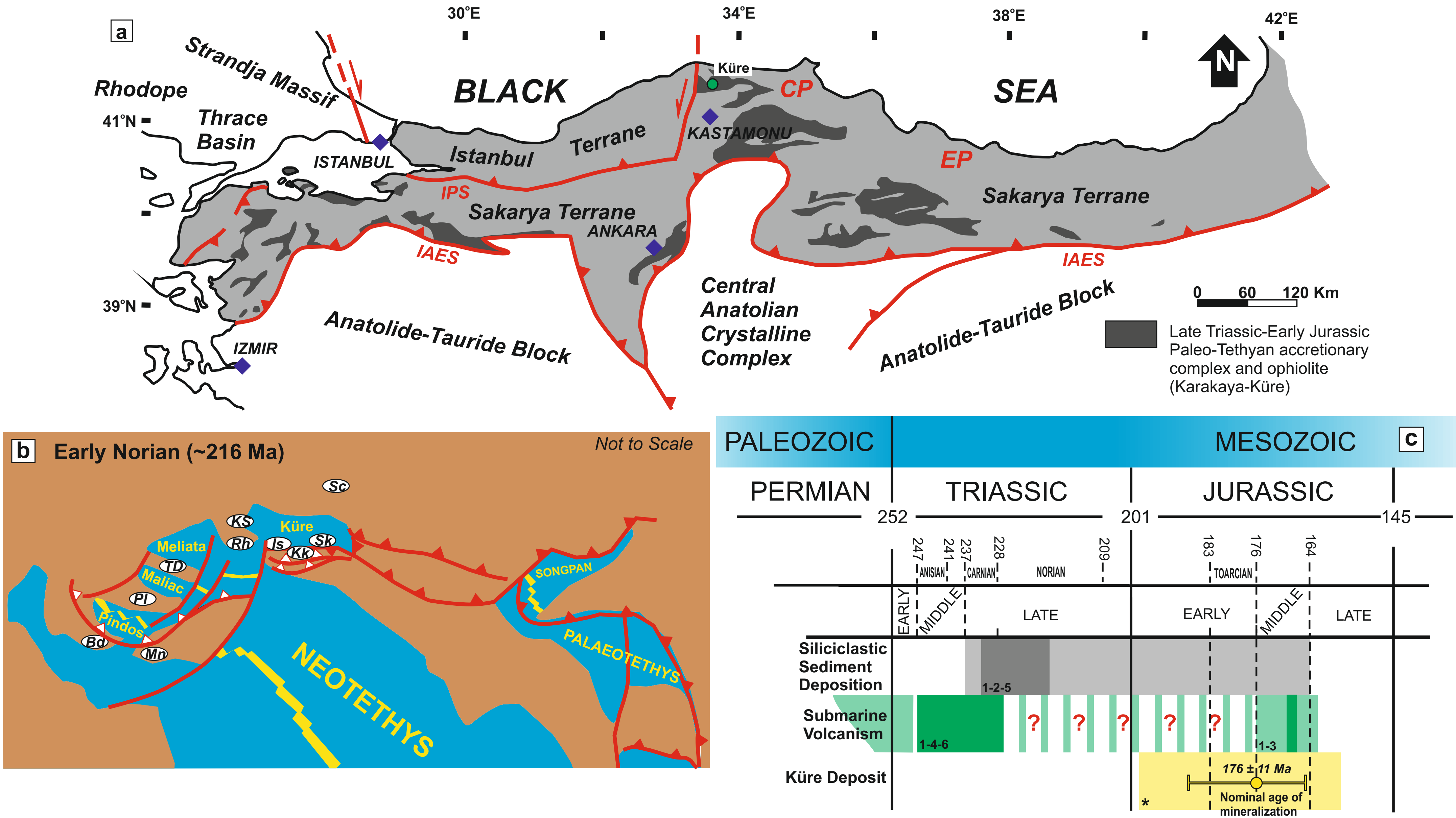

Table 1

Table 1

Element	*Pyrite*						*Chalcopyrite*						*Sphalerite*					*L.O.D.**
wt %	**9-2**	**9-10**	**9-12**	**9-4**	**5B-10**	**6BA-14**	**9-14**	**9-7**	**9-6**	**4A-20**	**5B-6**	**5B-12**	**9-5**	**5B-19**	**5B-20**	**5B-21**	**5B-22**	**wt%**
S	53.72	53.66	52.92	53.33	53.23	52.93	34.87	34.97	34.96	35.25	34.65	35.68	33.28	33.17	32.87	32.98	33.18	*0.02*
Fe	45.20	46.97	45.62	46.39	46.47	46.62	29.95	29.85	30.21	31.00	30.23	31.31	5.55	3.80	2.41	2.58	2.70	*0.08*
Ni	0.00	0.00	0.02	0.01	0.00	0.01	0.00	0.00	0.00	0.00	0.01	0.00	0.00	0.00	0.02	0.00	0.04	*0.04*
Zn	0.04	0.11	0.00	0.31	0.00	0.00	0.00	0.08	0.21	0.00	0.00	0.00	56.66	59.51	62.45	61.41	62.06	*0.08*
Cu	0.05	0.00	0.18	0.17	0.07	0.42	33.99	33.75	33.88	33.82	33.88	31.38	3.77	1.31	1.34	1.56	1.16	*0.09*
As	0.03	0.03	0.14	0.57	0.06	0.05	0.00	0.00	0.00	0.00	0.03	0.05	0.00	0.07	0.00	0.00	0.01	*0.07*
Se	0.01	0.01	0.00	0.05	0.05	0.00	0.02	0.00	0.01	0.02	0.00	0.00	0.00	0.00	0.00	0.03	0.01	*0.05*
Sb	0.00	0.00	0.02	0.00	0.00	0.00	0.00	0.00	0.00	0.00	0.00	0.00	0.13	0.02	0.00	0.00	0.02	*0.03*
Te	0.01	0.00	0.02	0.03	0.01	0.00	0.03	0.00	0.01	0.03	0.02	0.01	0.00	0.00	0.00	0.00	0.02	*0.06*
Cd	0.03	0.00	0.00	0.00	0.00	0.00	0.00	0.00	0.00	0.00	0.00	0.00	0.04	0.16	0.10	0.11	0.15	*0.02*
Co	1.39	0.00	0.64	0.69	0.45	0.00	0.00	0.00	0.00	0.00	0.00	0.00	0.05	0.05	0.05	0.06	0.02	*0.03*
Ag	0.00	0.01	0.02	0.01	0.05	0.09	0.13	0.04	0.00	0.00	0.00	0.00	0.05	0.00	0.02	0.00	0.06	*0.06*
Au	0.00	0.05	0.00	0.01	0.11	0.03	0.01	0.00	0.00	0.00	0.06	0.04	0.00	0.00	0.00	0.04	0.00	*0.09*
Pb	0.04	0.00	0.00	0.00	0.00	0.00	0.00	0.00	0.00	0.00	0.00	0.00	0.00	0.00	0.00	0.00	0.00	*0.01*
Bi	0.00	0.00	0.00	0.00	0.00	0.00	0.00	0.00	0.00	0.00	0.00	0.00	0.00	0.00	0.00	0.00	0.00	*0.01*
Total	*100.52*	*100.84*	*99.58*	*101.57*	*100.50*	*100.15*	*99.00*	*98.69*	*99.28*	*100.12*	*98.88*	*98.47*	*99.53*	*98.09*	*99.26*	*98.77*	*99.43*	
Zn/Cd	-	-	-	-	-	-	-	-	-	-	-	-	*1417*	*372*	*625*	*558*	*414*	

L.O.D.*: Averages of the limits of detection for all samples calculated by 3-sigma (3σ) approach.

Table 2

Table 2

No	$T_{m(ice)}$ (°C)	T_{fm} (°C)	T_h (°C)	Salinity (wt % NaCI)	Inclusion area (μm²)	Vapor area (μm²)	Vapor/ Liquid
Fluid inclusions population 1							
1	-3.0	-50.0	317.0	5.0	636.0	118.0	0.19
2	-2.0	-43.0	270.9	3.4	608.0	115.0	0.19
3	-3.0	-59.0	209.0	5.0	1496.0	253.7	0.17
4	-1.0	-53.0	309.0	1.7	1543.0	203.0	0.13
5	-	-	292.0	-	-	-	-
6	-	-	315.0	-	-	-	-
7	-1.3	-36.0	284.5	2.2	2182.0	613.0	0.28
8	-0.9	-53.2	298.4	1.6	2200.0	610.0	0.28
9	-0.9	-55.5	317.5	1.6	782.0	145.0	0.19
10	-0.5	-54.0	305.7	0.9	-	-	-
11	-	-	273.6	-	-	-	-
12	-1.1	-30.0	285.8	1.9	1073.0	218.0	0.20
Mean	-1.5	-48.2	289.9	2.6	1315.0	284.5	0.20
Median	-1.1	-53.0	295.2	1.9	1284.5	210.5	0.19
Fluid inclusions population 2							
1	-2.4	-43.0	224.0	4.0	608.0	81.0	0.13
2	-1.2	-44.0	161.5	2.1	1763.0	74.0	0.04
3	-	-	245.7	-	3763.0	139.0	0.04
4	-	-	245.2	-	-	-	-
5	-	-	209.5	-	-	-	-
6	-1.7	-34.0	212.4	2.9	1191.0	172.0	0.14
7	-1.3	-	187.2	2.2	-	-	-
8	-1.7	-33.9	169.7	2.9	3974.0	431.0	0.11
9	-1.7	-31.0	168.0	2.9	1202.0	105.0	0.09
Mean	-1.7	-37.2	202.6	2.8	2083.5	167.0	0.09
Median	-1.7	-34.0	209.5	2.9	1482.5	122.0	0.10

(T_h): homogenization temperature; **(T_{fm}):** initial/first melting temperature; $T_{m(ice)}$: final ice melting temperature.

Table 3

Table 3

Sample No.	Lithology/ Sample Type	Re ppb	± 2SE	Os ppt	± 2SE	^{187}Re ppb	± 2SE	$^{187}Os^r$ ppt	± 2SE	%$^{187}Os^r$	± 2SE	%$^{187}Os^r$ (*)	$^{187}Re/^{188}Os$	± 2SE	$^{187}Os/^{188}Os$	± 2SE	rho	model age Ma	± 2SE	Initial $^{187}Os/^{188}Os$ @ 180 Ma
M256/M1	massive ore/ drill core	336.2	1.2	598.5	272.0	211.3	0.8	595.0	86.4	102.4	14.9	99.2	90711.9	30014.6	249.4	82.5	1.000	168.8	24.5	-
M256/V1	stockwork ore/ drill core	*188.2*	*0.7*	*273.3*	*810.3*	*118.3*	*0.4*	*272.7*	*14.2*	*100.8*	*5.3*	-	*329370.4*	*697380.1*	*753.2*	*1594.8*	*1.000*	*138.2*	*7.2*	-
BK-US	disseminated ore/ outcrop	*225.6*	*0.8*	*760.5*	*1746.4*	*141.8*	*0.5*	*759.8*	*88.6*	*100.4*	*16.4*	-	*302350.7*	*492599.8*	*1614.1*	*2636.3*	*0.998*	*320.8*	*37.4*	-
KGT-3	massive ore/ drift	132.9	0.5	250.6	137.2	83.5	0.3	247.8	69.5	104.7	29.4	98.4	44545.1	18248.2	126.1	51.7	1.000	177.8	49.9	-
KGT-4	massive ore/ drift	147.3	0.5	286.5	145.1	92.6	0.3	283.4	75.7	104.5	27.9	98.5	45312.2	17134.1	132.7	50.2	1.000	183.4	49.0	-
KGT-5	massive ore/ drift	630.9	2.3	1175.2	535.7	396.6	1.4	1171.6	87.2	101.2	7.5	99.6	168744.0	55202.9	492.5	161.1	1.000	177.1	13.2	-
M256-S2-2	black shale/ drill core	1.15	0.01	195.5	2.0	-	-	-	-	-		-	29.9	0.6	0.5402	0.02	0.677	-	-	0.45
M256-S2-6	black shale/ drill core	0.63	0.01	157.5	1.6	-	-	-	-	-		-	20.1	0.5	0.5171	0.01	0.633	-	-	0.46

All ore samples are pyrite-rich sulfide concentrates. (*): Calculated with an initial of 2±68 as derived from the isochron.